

Recent Progress of Electrochemical Production of Hydrogen Peroxide by Two-Electron Oxygen Reduction Reaction

Nan Wang, Shaobo Ma,* Pengjian Zuo,* Jizhou Duan,* and Baorong Hou

Shifting electrochemical oxygen reduction reaction (ORR) via two-electron pathway becomes increasingly crucial as an alternative/green method for hydrogen peroxide (H_2O_2) generation. Here, the development of 2e^- ORR catalysts in recent years is reviewed, in aspects of reaction mechanism exploration, types of high-performance catalysts, factors to influence catalytic performance, and potential applications of 2e^- ORR. Based on the previous theoretical and experimental studies, the underlying 2e^- ORR catalytic mechanism is firstly unveiled, in aspect of reaction pathway, thermodynamic free energy diagram, limiting potential, and volcano plots. Then, various types of efficient catalysts for producing H_2O_2 via 2e^- ORR pathway are summarized. Additionally, the catalytic active sites and factors to influence catalysts' performance, such as electronic structure, carbon defect, functional groups (O, N, B, S, F etc.), synergistic effect, and others (pH, pore structure, steric hindrance effect, etc.) are discussed. The H_2O_2 electrogeneration via 2e^- ORR also has various potential applications in wastewater treatment, disinfection, organics degradation, and energy storage. Finally, potential future directions and prospects in 2e^- ORR catalysts for electrochemically producing H_2O_2 are examined. These insights may help develop highly active/selective 2e^- ORR catalysts and shape the potential application of this electrochemical H_2O_2 producing method.

anthraquinone oxidation–reduction.^[2] However, this multistep synthesis method generally requires complex large-scale infrastructure and expensive palladium hydrogenation catalysts, which also generates a substantial volume of organic byproduct wastes. The direct synthesis of H_2O_2 from hydrogen and oxygen provides a more straightforward and atom-economic process, to ideally solve the issues associated with the complex anthraquinone route.^[3] Nevertheless, this direct synthesis method generally needs the use of platinum-group noble-metal catalysts with low catalytic efficiency and faces the potential explosion hazard of oxygen/hydrogen mixtures, which make its commercial application doubtful. Another attractive and alternative route for the on-site direct production of H_2O_2 is an electrochemical process, which can ideally solve the issues associated with the indirect anthraquinone route and direct synthesis of H_2O_2 from H_2 and O_2 .^[4] The electrochemical production of H_2O_2 can be realized mainly through two pathways, including the 2e^- oxygen reduction and water

oxidation. In this paper, the H_2O_2 generation via 2e^- oxygen reduction pathway will be discussed in detail.

Molecular oxygen generally can be electrochemically reduced to H_2O via a 4e^- transferred pathway, or H_2O_2 with 2e^- pathway in aqueous solution.^[5] Substantial efforts in recent years have aimed at efficiently generating electricity simultaneously with a high-yield production of H_2O_2 . In the 1930s, Berl firstly reported to produce H_2O_2 through electrochemical reduction of oxygen,


1. Introduction

H_2O_2 is a valuable oxidative chemical with rapidly growing demand in various applications, including the chemical synthesis, pulp/paper bleaching, and wastewater treatment (organic pollutants degradation/drinking water purification).^[1] The current industrial scale synthesis of H_2O_2 involves an energy-intensive

Dr. N. Wang, Prof. J. Duan, Prof. B. Hou
Key Laboratory of Marine Environmental Corrosion and Bio-Fouling
Institute of Oceanology
Chinese Academy of Sciences
7 Nanhai Road, Qingdao 266071, China
E-mail: duanjz@qdio.ac.cn

Dr. N. Wang, Prof. J. Duan, Prof. B. Hou
Center for Ocean Mega-Science
Chinese Academy of Sciences
7 Nanhai Road, Qingdao 266071, China
Dr. N. Wang, Prof. J. Duan, Prof. B. Hou
Open Studio for Marine Corrosion and Protection
Pilot National Laboratory for Marine Science and Technology (Qingdao)
1 Wenhai Road, Qingdao 266237, China

Dr. S. Ma, Prof. P. Zuo
MITT Key Laboratory of Critical Materials Technology for New Energy
Conversion and Storage
School of Chemistry and Chemical Engineering
Harbin Institute of Technology
Harbin 150001, China
E-mail: shaobomahit@gmail.com; zuopj@hit.edu.cn

 The ORCID identification number(s) for the author(s) of this article can be found under <https://doi.org/10.1002/advs.202100076>

© 2021 The Authors. Advanced Science published by Wiley-VCH GmbH. This is an open access article under the terms of the Creative Commons Attribution License, which permits use, distribution and reproduction in any medium, provided the original work is properly cited.

DOI: 10.1002/advs.202100076

which was further adopted to produce dilute alkaline H_2O_2 via the well-known Huron–Dow process.^[6] The Huron–Dow process was commercialized in 1991, due to that the produced dilute alkaline H_2O_2 could be directly used for pulp and paper bleaching process.^[6] However, the Huron–Dow process can only produce low-purity and high alkalinity H_2O_2 solution product, which not work in acid and neutral solution. Recently, the electro-Fenton process, based on a mixture of electrochemical produced H_2O_2 and Fe^{2+} ion, is widely studied to produce hydroxyl radicals ($\cdot\text{OH}$), which can be further used to degrade organic pollutants.^[1a] Microbial electrochemical cell, constructed with microbes containing anode and acetate (waste-water) electrolyte, can also produce H_2O_2 at cathode side, while it always exhibits a lower catalytic efficiency.^[7] For the $2e^-$ ORR route to generate H_2O_2 , exploring electrocatalysts with high activity and selectivity in acid/neutral/alkaline electrolyte is prerequisite. Until now, a variety of materials are investigated as $2e^-$ ORR catalysts, such as noble metal/alloys, functional (O, N, F, S, or B doped) carbon materials, non-noble transition metals, single-atom catalysts (SACs) and molecular complexes.^[8] However, the reported catalysts still face the unsatisfactory catalytic performances. There is still a long way to realize the large-scale production of H_2O_2 via electrochemical $2e^-$ ORR pathway. The critical knob for exploring efficient catalysts relies on the proper binding strength between the reaction catalytic sites and oxygen/oxygen transition species. A too-strong interaction may easily dissociate the O_2 molecule toward H_2O via $4e^-$ pathway, while a too-weak interaction may cause a high selectivity to H_2O_2 but lower catalytic activity.^[5a] Therefore, an ideal $2e^-$ ORR electrocatalyst with flexible tenability in electronic structures is highly desired for systematic control of $2e^-$ ORR pathways as well as improvements in catalytic activities.

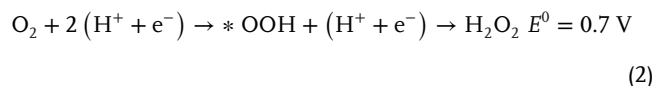
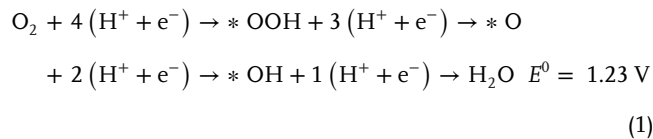
In this review, we summarized the development of two-electron electrochemical ORR catalysts in recent years, in aspects of catalytic mechanism, types of high-performance catalysts, factors to influence catalytic performance and potential applications (Figure 1). Until now, a diverse range of electrochemical catalysts are investigated for the electrochemical synthesis of H_2O_2 , such as noble metal/alloys, modified carbon materials, non-noble transition metals, single-atom catalysts and molecular complexes. Various factors are elucidated to influence the catalytic performance of H_2O_2 electrogeneration, including electronic structure, carbon defect, functional groups (O, N, B, S, F, etc.), synergistic effect, pH, pore structure, and steric hindrance effect. Additionally, the electrochemical synthesis of H_2O_2 exhibits attractive potential applications, containing disinfection, organics degradation, wastewater treatment, and energy storage. Based on the current researches and crucial challenges of $2e^-$ ORR, we further proposed the further development of $2e^-$ ORR, including mechanism exploring, rational design of catalysts, catalytic activity optimization in various electrolytes and potential applications.

2. Catalytic Mechanism of $2e^-$ ORR to H_2O_2

2.1. Reaction Pathway and Free Energy Diagram

The electrochemical oxygen reduction reaction always includes two kinds of reaction pathways. The first one is $4e^-$ associative reaction pathway, as shown in Equation (1), which involves four primitive steps and three different reaction intermediates,

namely $\ast\text{OOH}$, $\ast\text{O}$, and $\ast\text{OH}$, respectively. The second one is $2e^-$ associative pathway, corresponding to partial reduction of oxygen to H_2O_2 , which contains two primitive steps and only one $\text{OOH}\ast$ reaction intermediate (Equation (2)). The catalytic activity and selectivity of the catalysts toward H_2O_2 production are mainly determined by the binding free energy of $\ast\text{OOH}$ intermediate ($\Delta G(\ast\text{OOH})$)



In the oxygen reduction process, there is an obvious competition between $4e^-$ reaction pathway and $2e^-$ reaction pathway (Figure 2a). Specifically, hydroperoxide species have three possible subsequent pathways, 1) diffuse directly into the electrolyte as final product, 2) further electrochemically reduced to OH^- via $4e^-$ pathway, 3) chemically decomposed to O_2 and OH^- . As H_2O is the thermodynamically favored product, it is an obstacle for synthesizing H_2O_2 product via $2e^-$ ORR pathway. As shown in Figure 2a, the $\ast\text{OOH}$ is the common intermediate between the two ORR pathways, and the bond strength between catalysts and $\ast\text{OOH}$ intermediate determines the reaction product. Thus, the final product of the ORR process strongly depends on the electrochemical catalysts.

Density functional theory (DFT) calculations work well in describing adsorption energies of intermediates on catalysts surface, except the energy of the solvated protons and the electrons in the electrode at a given potential. Nørskov et al. firstly developed a typical calculation method upon the catalytic process, based on computational hydrogen electrode (CHE) model. The free energy of a single proton–electron pair is defined as $-eU$ relative to H_2 in the gas phase at standard conditions, where U is the electrode potential versus the reversible hydrogen electrode (RHE).^[9] The adsorption free energy of an intermediate (with n proton–electron pairs) generally consists of several parts, including calculated binding energy (ΔE_{ele}), adsorbate solvation (ΔE_{w}), electric field effects (ΔE_{field}), zero-point energy (ΔE_{ZPE}) and entropic corrections ($-T\Delta S$), as displayed in Equation (3)

$$\Delta G = \Delta E_{\text{ele}} + \Delta E_{\text{w}} + \Delta E_{\text{field}} + \Delta E_{\text{ZPE}} - T\Delta S - neU \quad (3)$$

Figure 2b shows the DFT-calculated free energy diagram of Pt-Hg_4 for the $2e^-$ ORR process using the CHE model. At $U = 0.0 \text{ V}$ (blue lines), all the reaction steps are downhill, indicating it is a facile reaction at this state. The green line represents the thermodynamics free energy of sole $\ast\text{OOH}$ intermediate at the equilibrium potential ($U = 0.7 \text{ V}$), and the adsorption energies are shifted by $-neU$ based on Equation. Figure 2b shows that the reduction of O_2 to $\ast\text{OOH}$ is uphill in energy at $U = 0.7 \text{ V}$ (green lines), implying this limiting reaction step may hinder further adsorption and dissociation of O_2 . Based on the CHE model, the thermodynamic limiting potential (U_{L}) is defined as the highest

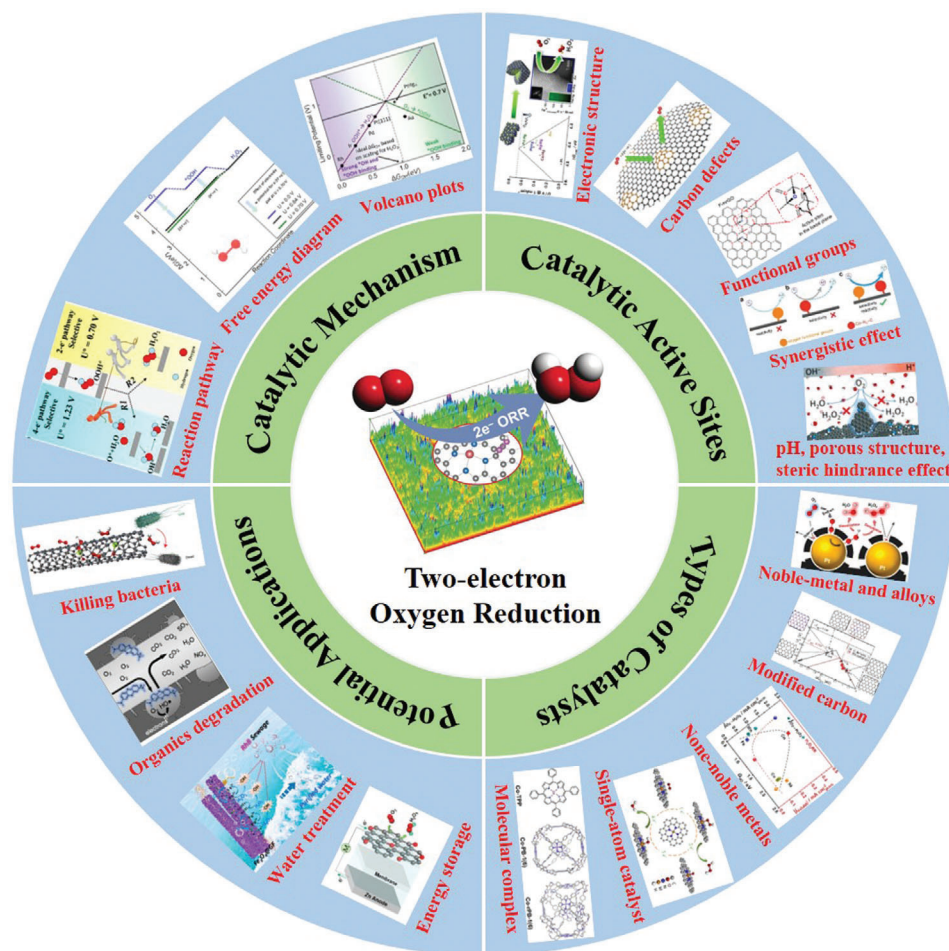


Figure 1. Schematic diagram of $2e^-$ ORR electrochemical catalysts summarized in this review, including catalytic mechanism, catalytic active sites, types of catalysts and potential applications. Reaction pathway: Reproduced with permission.^[12] Copyright 2019, American Chemical Society. Free energy diagram and volcano plots: Reproduced with permission.^[5a] Copyright 2018, American Chemical Society. Electronic structure: Reproduced with permission.^[9a] Copyright 2014, American Chemical Society. Carbon defects: Reproduced with permission.^[43] Copyright 2018, American Chemical Society. Functional groups: Reproduced with permission.^[55] Copyright 2018, Springer Nature. Synergistic effect: Reproduced with permission.^[65] Copyright 2019, Wiley-VCH. Porous structure: Reproduced with permission.^[66] Copyright 2014, American Chemical Society. Noble-metal and alloys: Reproduced with permission.^[23a] Copyright 2014, American Chemical Society. Modified carbon: Reproduced with permission.^[40a] Copyright 2018, American Chemical Society. None-noble metals: Reproduced with permission.^[16] Copyright 2019, American Chemical Society. Single-atom catalyst: Reproduced with permission.^[17] Copyright 2020, American Chemical Society. Molecular complex: Reproduced with permission.^[95] Copyright 2020, Wiley-VCH. Energy storage: Reproduced with permission.^[88] Copyright 2019, Springer Nature. Water treatment: Reproduced with permission.^[78] Copyright 2019, Elsevier. Organics degradation: Reproduced with permission.^[118] Copyright 2019, American Chemical Society. Killing bacteria: Reproduced with permission.^[122] Copyright 2018, American Chemical Society. Center image: Reproduced with permission.^[86] Copyright 2020, Wiley-VCH.

potential, at which all the reaction steps are downhill in free energy. The calculated U_L of Pt–Hg₄ catalyst is 0.64 V, and free energy diagram at U_L is displayed as black line in Figure 2b. The difference between the equilibrium potential and the U_L is defined as theoretical overpotential (η_{theo}), and the $\eta_{\text{theo}} \approx 0.7\text{--}0.63\text{ V} = 0.07\text{ V}$ for Pt–Hg₄.

2.2. Kinetics and Volcano Plots for $2e^-$ ORR to H₂O₂

As noted earlier, the $2e^-$ ORR catalysts generally are also active for generation of water (thermodynamically favorable product). As the free diagram in Figure 2c, the key to avoid the $4e^-$ pathway is to prevent the O–O bond dissociation in the adsorbed *OOH.

Thus, the catalysts with strong oxygen binding energies (favorable *O formation) are not suitable for $2e^-$ ORR, which limits the search to weak oxygen binding catalysts.^[5a] Additionally, suitable adsorption energy of *OOH on catalysts is also essential to achieve the high catalytic activity. For the $2e^-$ ORR catalytic process, the reaction pathway mainly consists of two steps, corresponding to the generation and removal of sole *OOH intermediate on the catalysts surface. Hence, the theoretical overpotential can be only determined as a function of the *OOH binding energy. A critical determining factor is whether the catalyst can dissociate the O–O bond, and the weak adsorption of intermediate will lead to high H₂O₂ selectivity but low activity. On the basis of scaling relations between different descriptors, corresponding to $\Delta G(*\text{OOH}) = \Delta G(*\text{OH}) + 3.2$ and $\Delta G(*\text{O}) = 2\Delta G(*\text{OH})$, the

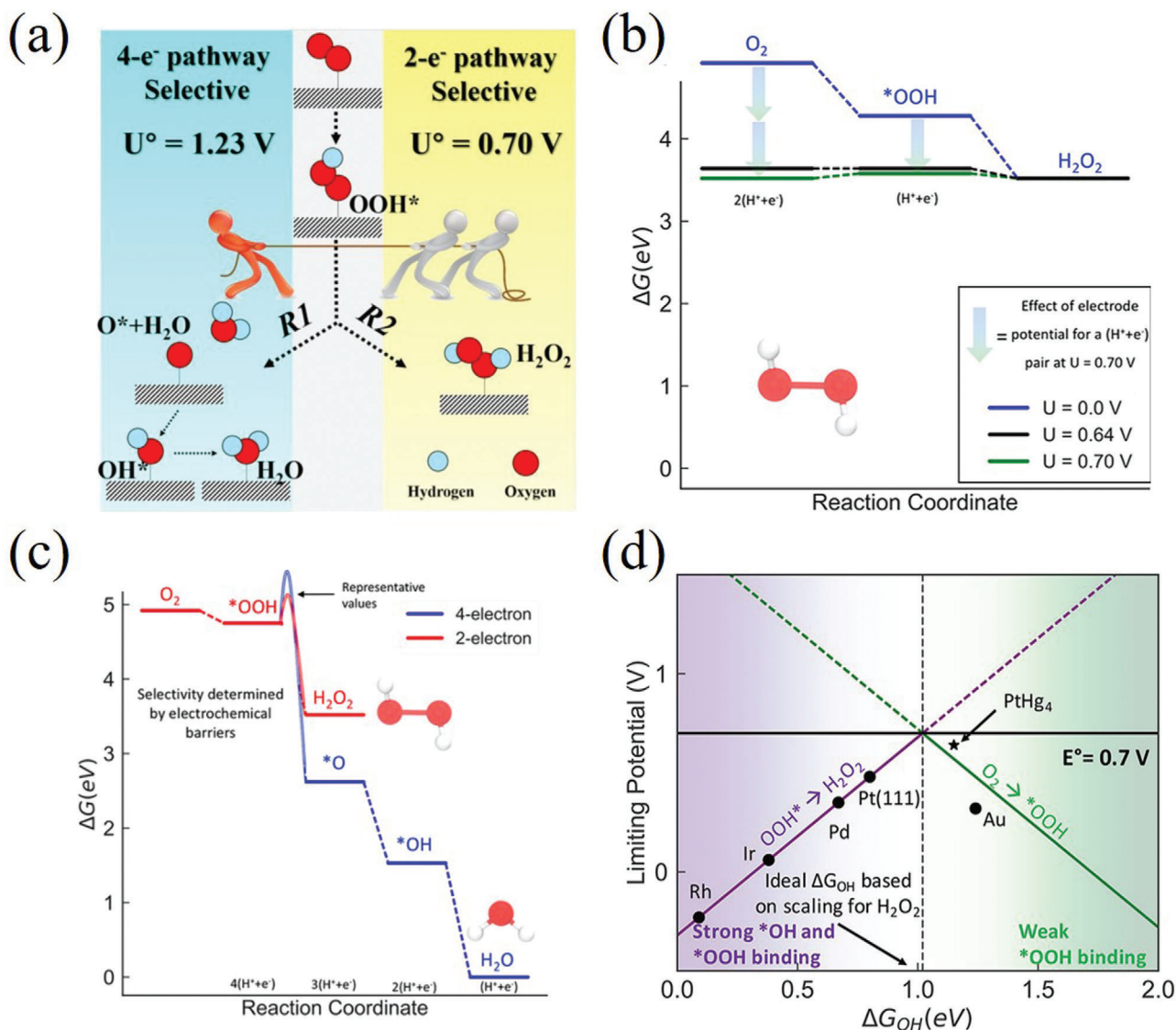


Figure 2. a) Schematic illustration of the reactions and the equilibrium potentials during the oxygen electrochemical reduction. Reproduced with permission.^[12] Copyright 2019, American Chemical Society. b) Free energy diagram of PtHg₄ on 2e⁻ ORR at three different potentials: 0 V (blue lines), the corresponding equilibrium potential (green lines), and the limiting potential (black lines). The blue-green arrows indicate the effect of the potential based on the RHE model. Reproduced with permission.^[13] Copyright 2013, Springer Nature. c) Free energy diagram for the four-electron (blue line) and two-electron (red line) oxygen reduction. The electrochemical barrier for the $*OOH$ to H_2O_2 or $*O$ are illustrative and indicate the importance of kinetics in determining catalyst selectivity. d) Limiting potentials for individual steps in Equations (4) and (5), showing the strongly bound $*OH$ region (solid purple line) and weakly bound $*OOH$ region (solid green line) for the 2e⁻ process. The color gradient indicates the strong $*OH$ and weak $*OOH$ binding regions. c,d) Reproduced with permission.^[5a] Copyright 2018, American Chemical Society.

limiting potentials for 2e⁻ ORR can be expressed using $*OH$ as a descriptor with the relationship as the Equations (4) and (5)

$$U_{L1} = -\Delta G_{*OH} + 1.72 \quad (4)$$

$$U_{L2} = \Delta G_{*OH} - 0.32 \quad (5)$$

Figure 2d presents the computed two-electron volcano relation between the limiting potentials and $\Delta G(*OH)$ for the individual steps in Equation (4) (green line) and Equation (5) (purple line).

The lowest limiting potential for the full catalytic reactions defines the overall limiting potential for the reaction, which is indicated by the purple and green solid lines. Because the catalytic process has only one $*OOH$ intermediate, those two curves cross at the peak of the volcano, corresponding to the equilibrium potential at 0.70 V. As such, it is possible, in principle, to design one electrochemical catalyst with an ideal activity near the peak of volcano, where the binding strength between $*OOH$ intermediate and catalyst is neither too weak nor too strong.^[10] As shown in Figure 2d, for catalysts with strong $*OOH$ (or $*OH$) bonding energy lying on the left side of the two-electron volcano (solid

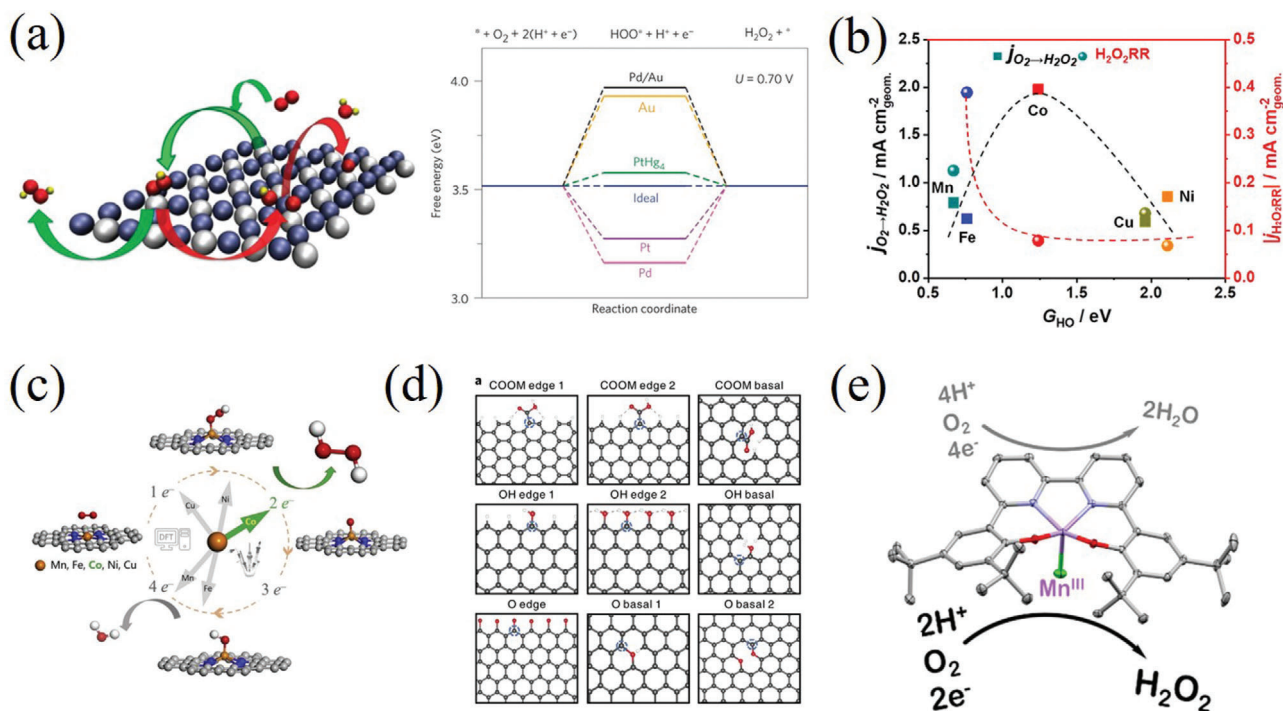


Figure 3. a) PdHg₄ catalyst and free-energy diagram of different catalysts for oxygen reduction to H₂O₂. Reproduced with permission.^[13] Copyright 2013, Springer Nature. b) Thermodynamic relations (volcano) lines for the two-electron ORR of M–N–C catalysts. Reproduced with permission.^[16] Copyright 2019, American Chemical Society. c) Co–N–C SAC for H₂O₂ production. Reproduced with permission.^[17] Copyright 2020, Elsevier. d) Oxidized carbon catalyst with different oxygen functional groups for 2e⁻ ORR. Reproduced with permission.^[15a] Copyright 2018, Springer Nature. e) Molecular manganese complex with a bipyrindine-containing Schiff base ligand catalyst. Reproduced with permission.^[15b] Copyright 2018, American Chemical Society.

purple line), *OOH→H₂O₂ is potential limiting step and four-electron ORR may dominates over the two-electron pathway; On the other hand, in the case of weak *OOH binding lying on the right side of the volcano (solid green line), O₂→*OOH is potential limiting step, which is expected to yield increased H₂O₂ selectivity but lower activity.^[11] As a result, the most promising catalyst with both high activity and selectivity toward H₂O₂ would be found at the apex of the 2e⁻ volcano plot.

3. Electrocatalysts and Factors Influencing 2e⁻ ORR Activity/Selectivity

For ideal 2e⁻ ORR catalysts, the adsorption of *OOH should be enhanced to achieve the high catalytic activity, while the adsorption of *O (the product of *OOH dissociation) should be reduced to obtain high selectivity.^[14] The electrocatalyst for the 2e⁻ reduction of oxygen should meet several criteria: high activity, operating with low catalyst loading, suitable conductivity, ideal mass transfer rate and high onset potentials/limiting diffusion current densities; high selectivity, ensuring high yields of H₂O₂ instead of H₂O; high stability, enabling long-term durability in various electrolytes. Earlier studies on 2e⁻ ORR to H₂O₂ generation mainly operated in alkaline solution, which can produce high alkalinity H₂O₂ solution for pulp and paper bleaching process. With the increasing application demand of H₂O₂, attractive electrochemical catalysts should also process well catalytic performance in acid and medium electrolyte.

To date, numerous materials, such as noble metals/alloys, functional (O, N, F, S, B⁻) carbons, non-noble transition metals, single-atom catalysts and molecular complex, have been proposed to improve the catalytic performance of 2e⁻ ORR.^[8a,15] Rossmeisl and co-workers reported Pt–Hg nanoparticles with ultrahigh catalytic performance for H₂O₂ production (Figure 3a).^[13] The isolated Pt atoms surrounded by inert Hg atoms can effectively adsorb *OOH as well as decrease the O* binding energy strength, as reflected by the adsorption energies of *OOH/*O falling below the scaling line of single elemental metals. Several bimetallic alloys, such as Pd–Au and Pd–Hg, also show impressive mass activity and high selectivity (>95%) toward the synthesis of H₂O₂.^[9a,14b] However, the scarcity of noble metals and toxicity of Hg significantly hinder their large-scale applications. The state of d-orbitals electrons in transition metals is also a crucial factor to affect the *OOH binding strength. Researchers screened out seven non-noble transition metal catalysts toward two-electron ORR with higher activity than the PtHg₄ in acid media, by means of DFT computations.^[8a,12] The DFT results displays the predicted binding energy of *OH intermediate over Co–N–C catalyst is located near the top of the volcano accounting for favorable two-electron ORR (Figure 3b).^[16] SAC is also a kind of attractive 2e⁻ ORR catalyst, due to its suitable binding energy between *OOH intermediate and high mass activity. As show in Figure 3c, Co SAC anchored in nitrogen-doped graphene can generate H₂O₂ via 2e⁻ ORR pathway with high catalytic efficiency.^[17] The support in SAC generally is crucial for active sites atomic dispersion and oxygen species

adsorption energy regulation.^[18] Carbon materials have widely served as low-cost and highly active $2e^-$ ORR electrocatalysts to yield H_2O_2 . As shown in Figure 3d, the surface oxidation approach can influence the structure of graphene catalyst, and the carbon atoms adjacent to oxygen functional groups (OFGs) (C–O–C and –COOH) are the active sites for $2e^-$ ORR to generate H_2O_2 .^[15a] The molecular complex also processes attractive electrocatalytic performance for producing H_2O_2 under aqueous conditions. As displayed in Figure 3e, the molecular manganese complex with bipyridine-containing Schiff base ligand exhibit high H_2O_2 catalytic performance with $81 \pm 4\%$ Faradaic efficiency.^[15b] Generally, the electronic structure, physical/chemical structure, active sites, and operation conditions of those catalysts can be well regulated. Each type of electrocatalysts and factors affecting the electrochemical performance will be discussed in detail in the following parts.

3.1. Noble-Metal Catalysts and Influence Factors

Noble-metals are the most promising electrocatalysts for producing H_2O_2 via $2e^-$ ORR, which generally exhibit advantages of small overpotentials, ultrahigh H_2O_2 selectivity (up to $\approx 98\%$) as well as high stability. Numerous noble-metal based catalysts, such as Au, Pd, and Pt, generally exhibit high catalytic performance for the electrochemical production of H_2O_2 . To improve $2e^-$ catalytic performance, most studies are mainly focusing on the structure regulation of noble-metal based catalysts, including electronic structure, particle size, types of support materials, defects and crystal grains, and functional groups. Besides the intrinsic electronic/crystalline structure of noble metals, several factors, such as alloying, particle size, mass loading, and interparticle distance, will influence the catalytic performance of the $2e^-$ ORR.

Various noble single metal catalysts, such as Au, Pd, and Pt, are investigated as the $2e^-$ ORR catalysts to produce H_2O_2 . Previously, many Au based materials, such as Au/C, Au/Vulcan XC-72R, and $Au_{25}(SC_{12}H_{25})_{18}$, were studied as promising catalysts toward selective H_2O_2 generation, and the electrochemical reaction mainly occurred on Au (111) and Au (110) active crystalline planes.^[19] Chang et al. reported a $Pd^{\delta+}$ -OCNT electrocatalyst with nearly 100% selectivity toward H_2O_2 electrochemical production and a high mass activity (1.946 A mg^{-1} at 0.45 V) in acidic electrolyte (Figure 4a).^[20] The X-ray absorption fine structure characterization and DFT calculations demonstrate that the synergistic interaction between partially oxidized Pd clusters and oxygen-functionalized CNT substrate is crucial for the high $2e^-$ ORR catalytic activity. Various other Pd/C catalysts displayed highly selectivity toward H_2O_2 production.^{[21][22]} Pt-based catalysts also process high $2e^-$ ORR catalytic performance.^[23] For instance, Choi et al. reported that sulfur doped carbon (17 wt% S) could stabilize high loading of platinum (5 wt%), which exhibited high H_2O_2 selectivity ($\approx 96\%$) via $2e^-$ ORR.^[23b]

Noble metal alloys, with synergetic presence of two (or more) metals with different oxygen binding energies, generally exhibit excellent electrochemical catalytic activity for $2e^-$ H_2O_2 production. Siahrostami et al. firstly reported that Pt–Hg nanoparticles exhibited ultrahigh catalytic activity for generating H_2O_2 , corresponding to selectivity up to 96% at 50 mV overpotential.^[13]

The inert Hg atoms could surround isolated Pt atoms and adjust the binding energy between oxygen species and catalytic sites. Jirkovský et al. indicted that alloying Pd, Pt or Rh atoms on Au surface could enhance the H_2O_2 production relative to pure Au by DFT modeling.^[24] Recently, Zheng et al. reported an Au–Pt–Ni NRs ternary metal catalyst, which exhibited high catalytic selectivity of 95% toward H_2O_2 production between 0.45 and 0.55 V (vs RHE) (Figure 4b).^[25] Lots of noble metal alloys, such as Pt–Au–Cu nanowire and Pd–Au, also reported as high efficient $2e^-$ ORR catalysts for H_2O_2 production.^[26] Although the noble-based catalysts generally process high $2e^-$ ORR catalytic performance in acid medium, the mass loading/mass activity of catalysts should be further optimized and the compatibility in alkaline/neutral electrolyte should be enhanced.

The crystalline/amorphous structure and particle size are the crucial factors to influence the catalytic performance of catalyst for $2e^-$ ORR. Kronawitter and co-workers reported the amorphous Pd nanoparticles exhibited an ultrahigh H_2O_2 selectivity above 95%, which was significantly higher than that of crystalline Pd catalyst (Figure 4c).^[21] Various studies demonstrate that the particle size of noble-metal clusters below $\approx 5 \text{ nm}$ always promotes high catalytic performance for $2e^-$ ORR.^[9a,19b,21,27] For instance, Anderson and co-workers prepared size-selected Pt_n clusters on indium tin oxide (ITO) composite, and the maximized H_2O_2 selectivity was observed with the smallest Pt_1 size species (Figure 4d).^[27] Jirkovský et al. discussed the effects particle size of Au nanoparticles on oxygen reduction selectivity for H_2O_2 production. The results showed that selectivity for H_2O_2 production was high for the catalyst with particle sizes below 6 nm.^[19b]

The loading amount, distinct interparticle distances of noble metal active sites and oxygen species adsorption direction are also crucial to the electrocatalytic activity and selectivity of H_2O_2 . It is demonstrated that a lower catalyst loading results in the sparse distribution of active sites and the dissociation of intermolecular O–O bond is hindered, which is beneficial to produce H_2O_2 via $2e^-$ ORR way.^[28] As shown in Figure 4e, on Pd–Au alloys with continuous Pd atom reactive sites, O_2 is adsorbed with “side-on” mode, which is conducive to O–O bond breakage and generation of H_2O .^[29] However, isolated Pd atom catalytic sites prefer the “end-on” binding mode for O_2 , which hinders O–O bond breakage such that H_2O_2 can be preferentially formed. Choi et al. demonstrated that controlled coating of Pt catalysts with amorphous carbon layers could induce selective end-on adsorption of O_2 on the Pt surface, which exhibited significantly enhanced H_2O_2 production selectivity up to 41%.^[23a] Fortunato et al. suggested that the catalysts with different Pd loadings and distinct interparticle distances could influence the catalytic performance toward H_2O_2 .^[22] As shown in Figure 4f, the generated H_2O_2 intermediate tends to diffuse into the electrolyte before further undergoing reduction to H_2O , when the Pd interparticle distance is higher than 125 nm.

3.2. Carbon-Based Catalysts and Influence Factors

Carbon based nanomaterials are recognized as promising $2e^-$ ORR electrocatalysts, due to the advantages of global abundance, low cost, high surface area, large pore volume, excellent

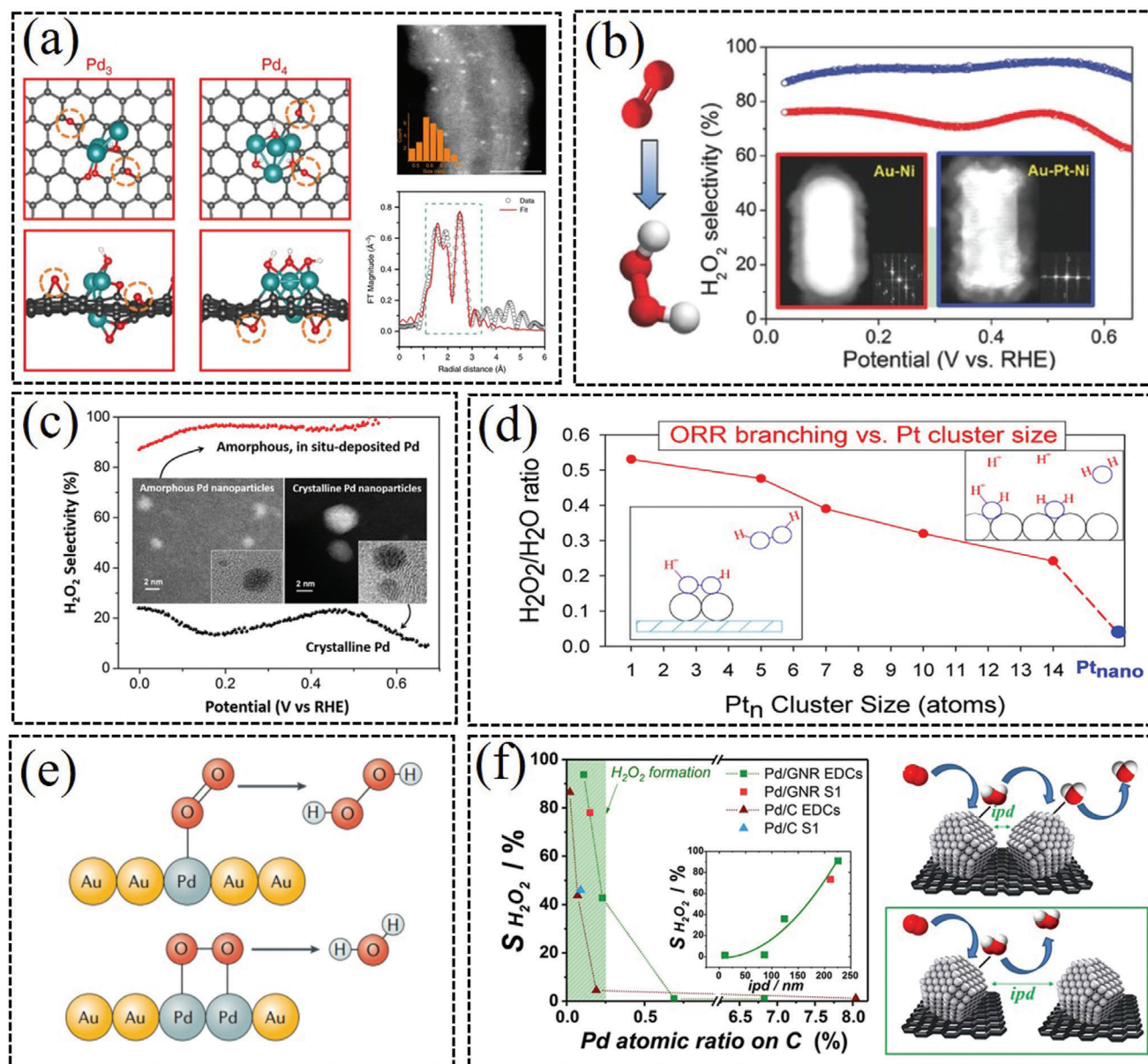


Figure 4. a) Promoting H_2O_2 production via 2e^- ORR by coordinating partially oxidized Pd and defect carbon. Reproduced with permission.^[20] Copyright 2020, Springer Nature. b) Au–Pt–Ni nanorods for high selectivity H_2O_2 production. Reproduced with permission.^[25] Copyright 2016, Wiley-VCH. c) The H_2O_2 catalytic selectivity of Pd nanoparticles with amorphous and crystalline structure. Reproduced with permission.^[21] Copyright 2019, American Chemical Society. d) Size-dependent properties of Pt_n/ITO catalyst. Reproduced with permission.^[27] Copyright 2015, American Chemical Society. e) The “end on” and “side on” adsorption mode of oxygen to Pd–Au alloys. Reproduced with permission.^[29] Copyright 2019, Springer Nature. f) The catalytic performance of Pd/C with distinct interparticle distances. Reproduced with permission.^[22] Copyright 2018, American Chemical Society.

stability, and good electrical conductivity.^[30] Some commercial porous carbon-based materials, such as Vulcan XC-72R,^[31] CMK-3,^[32] carbon black,^[33] and Printex L6,^[34] exhibit high practical application prospects for H_2O_2 generation via electrochemical 2e^- ORR pathway. Various synthesized porous carbon materials, including graphite felt,^[35] nanotubes,^[36] hierarchically porous carbon,^[37] and redox modifiers (quinones and azo compounds),^[38] also display 2e^- ORR catalytic performance to yield H_2O_2 under acidic/neutral/alkaline conditions. The pure carbon catalysts generally process unideal catalytic performance,

so structural reconstruction^[39] and heteroatom doping (O, N, F, S, P, and B)^[40] are useful strategies to boosting their 2e^- ORR catalytic performance. The catalytic performances of some carbon-based catalysts are listed in Table 1. Several crucial factors may influence the catalytic performances of catalysts, which include carbon defect, oxygen functional groups, nitrogen types, synergistic effect, and others (pH, applied potential, pore structure, and steric hindrance effect). In the following sections, we will discuss in detail the crucial factors that influence electrochemical performance of carbon-based catalysts.

Table 1. The electrochemical catalytic performance of some carbon-based catalysts.

Electrocatalysts	Electrolytes	H ₂ O ₂ [%]	E _{onset} vs RHE	N	Reference
CMK-3	0.1 M KOH	90	≈0.80 V	2.2	[41]
rGO-KOH	0.1 M KOH	≈100	≈0.8 V	≈2.0	[42]
Meso-C	0.1 M KOH	≈100	≈0.7 V	≈2.0	[43]
Meso-BMP-800	0.1 M HClO ₄ 0.5 M H ₂ SO ₄ + 0.05 M Na ₂ SO ₄	65.295	≈0.60 V≈0.70 V	≈2.72.1	[39a]
O-doped CMK3	0.1 M K ₂ SO ₄ 0.1 M KOH	7890	≈0.45 V≈0.8 V	≈2.4≈2.2	[32]
MNCs	0.5 M H ₂ SO ₄	90	≈0.5 V	2.2	[44]
Porous carbon	0.1 M Na ₂ SO ₄ + 0.5 M H ₂ SO ₄	82.4	≈0.60 V	≈2.4	[37]
N-doped graphitized carbon	0.1 M H ₂ SO ₄ 0.1 M NaOH	8040	0.4 V 0.71 V	2.43.2	[40b]
GOMC	0.1 M KOH	>90	0.81 V	≈2.2	[45]
NCA-850	0.1 M KOH	≈100	≈0.8 V	≈2.0	[46]
O-CNTs	0.1 M PBS 0.1 M KOH	≈85≈90	≈0.60 V≈0.80 V	≈2.3≈2.2	[15a]
Oxo-G	0.1 M KOH	>82	≈0.8 V	≈2.3	[47]
N-rGO	0.1 M KOH	–	≈0.75 V	–	[48]
NF-Cs	0.5 M H ₂ SO ₄ 0.1 M KOH	85–8889.6	0.7 V 0.8 V	2.32.2	[49]
N-doped C	0.1 M KOH	93	0.88 V	≈2.1	[50]
N-doped CMK3_800T	0.5 M H ₂ SO ₄ 0.1 M K ₂ SO ₄	98.589.8	0.49 V 0.52 V	2.02.1	[51]
N-doped C	0.5 M H ₂ SO ₄ 0.1 M K ₂ SO ₄ 0.1 M KOH	858595–98	≈0.40 V≈0.45 V 0.78 V	2.32.32.1	[39b]
Graphitic N–C	0.1 M KOH	75	0.74 V	≈2.5	[52]
2,2'-Dipyridylamine	0.5 M H ₂ SO ₄	≈80	≈0.6 V	2.4	[53]
N,S-MC	0.5 M H ₂ SO ₄ 0.5 M KOH	7675	≈0.32 V≈0.56 V	2.52.5	[40e]
N-MCs	0.1 M KOH	85	–	2.3	[54]
FPC	0.1 M Na ₂ SO ₄ + 0.05 M H ₂ SO ₄	93.6	≈0.3 V	≈2.1	[14b]
F-mrGO(600)	0.1 M KOH	≈100	0.78 V	≈2.0	[55]

3.2.1. Carbon Defects

Substantial investigations have demonstrated that the carbon defects exhibit high 2e[−] ORR catalytic activities, because the changes of geometrical and electronic structures can affect the binding strength of *OOH intermediate and the breaking energy of O–O bond.^[54,56] For instance, Bao et al. prepared the microporous and mesoporous carbon catalysts, which exhibit a high onset potential near the thermodynamic equilibrium potential (0.7 V vs RHE) and a high selectivity of >70% for H₂O₂ (Figure 5a).^[43] DFT calculation results demonstrate that various types of carbon defects in model graphene systems, including pentagon edges, single vacancies as well as double vacancies, are associated with catalytic performance for the 2e[−] ORR. McCloskey et al. elucidated the influence of carbon defects to the 2e[−] ORR catalytic performance (Figure 5b).^[48] They suggested that certain carbon defects associated with epoxy or ether groups have more pivotal role in promoting electrogeneration of H₂O₂ than other functionalities, such as nitrogen defects and carboxylic acid edge sites. Cohen-Karni and co-workers reported the nanowire-templated 3D fuzzy graphene, with abundant carbonyl (C=O) and hydroxyl (C–OH) groups edge defectives, which exhibited notable 2e[−] ORR catalytic efficiency (Figure 5c).^[57] They proposed that multiple functionalized configurations at both armchair and zigzag edges may achieve a local coordination environment for high efficiency 2e[−] ORR. Eigler and co-workers reported that the density of defects, including functionalization defects, carbon lattice defects, and nitrogen doping defects, were vital

for regulating 2e[−] ORR catalytic performance of the carbon catalysts (Figure 5d).^[47] Though defective carbons have shown good electrocatalytic performance toward H₂O₂, numerous defect-site structures will be formed during preparation. Thus, it is a challenge for selectively tailoring synthetic method to induce the formation of the most active/selective active-sites structure.

3.2.2. Oxygen Functional Groups

Recently, OFGs, such as C=O, C–O and COOH, are identified to sufficiently enhance the catalytic activity and selectivity for H₂O₂ electrochemical synthesis via 2e[−] ORR.^[58] Cui et al. observed that the oxidized carbon nanotubes (O-CNTs) exhibited both high catalytic activity and selectivity (≈90%) for H₂O₂ production via electrochemical 2e[−] ORR, and the catalytic properties were positively correlated with the oxygen content of the catalysts (Figure 6a).^[15a] The DFT calculation indicates the carbon atoms adjacent to oxygen functional groups (–COOH and C–O–C) are the active sites for the 2e[−] ORR. Recently, Guo et al. reported OFGs containing carbon-based catalyst by in situ engineering with cationic surfactant, which delivered a high peroxide production with a sustainably high selectivity (96%) over 10 h (Figure 6b).^[59] The prepared catalyst contains abundant surface carboxylates (–COO[−]) and surface carbonyls (–C=O) functional groups. The surface COO[−] groups are the main active sites with weak binding to surface peroxides, while surface C=O groups deteriorate selectivity by the strong binding with H₂O₂. Zhang et al. reported an air

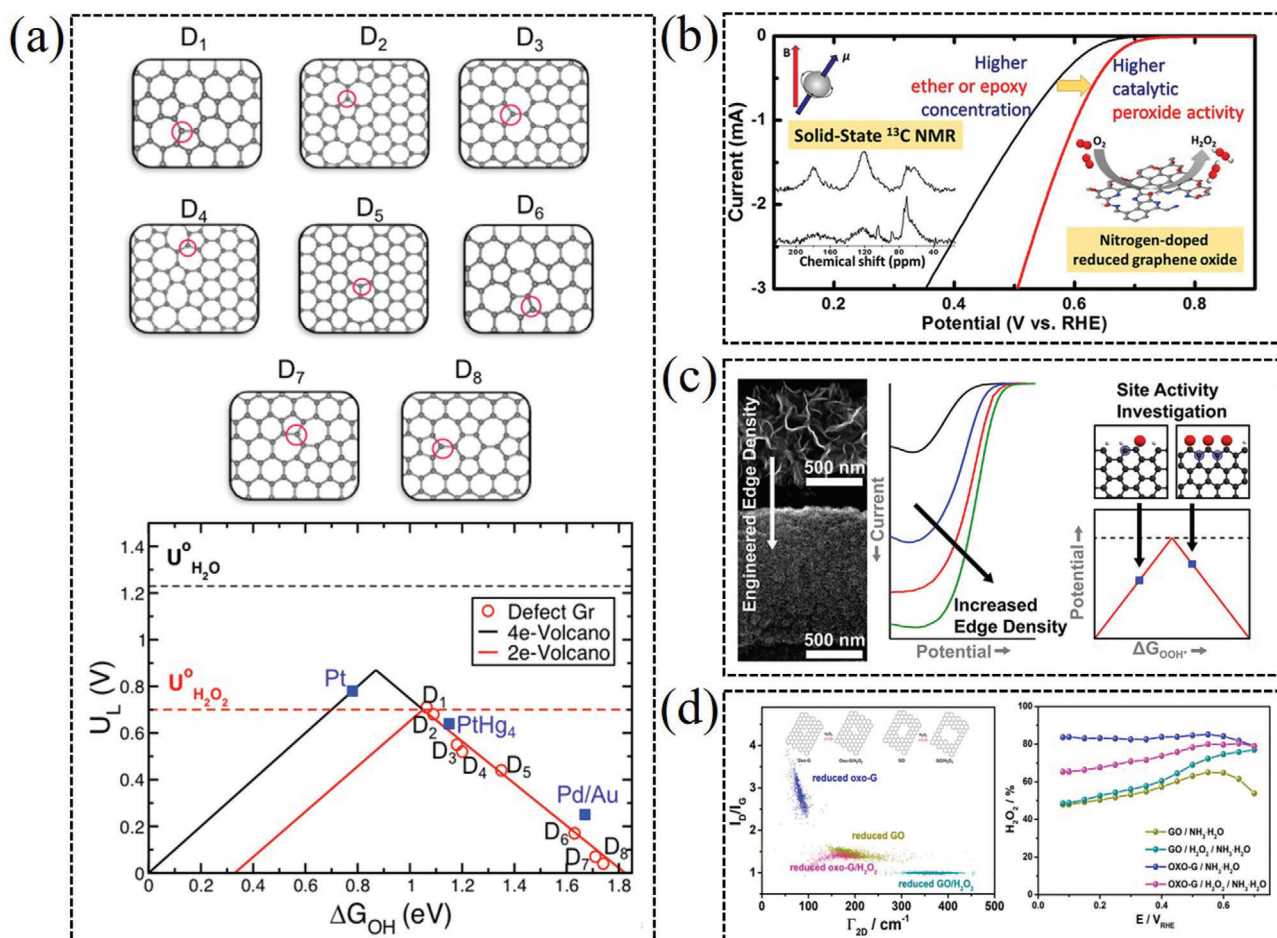


Figure 5. a) Different carbon defect type configurations examined in the DFT and two-electron (red)/four-electron (black) ORR-related volcano plots. Reproduced with permission.^[43] Copyright 2018, American Chemical Society. b) Carbon defects with higher ether or epoxy for peroxide generation. Reproduced with permission.^[48] Copyright 2019, American Chemical Society. c) 3D out-of-plane graphene edge sites for highly selective 2e⁻ ORR electrocatalysis. Reproduced with permission.^[57] Copyright 2020, American Chemical Society. d) In-plane carbon lattice-defect of nitrogen-doped graphene regulating electrocatalysis to H₂O₂ production. Reproduced with permission.^[47] Copyright 2019, American Chemical Society.

calcination method to improve the 2e⁻ ORR catalytic activity of commercial carbon black, in which OFGs exhibited main catalytic activity toward 2e⁻ ORR (Figure 6c).^[33b]

Although the introducing of oxygen functional groups generally can improve the 2e⁻ ORR catalytic performance of catalysts, the accurate catalytic active sites are always controversial and crucial for further studies. McCloskey et al. demonstrated a mild thermal reduced graphene oxide (mrGO) electrocatalyst for efficient H₂O₂ production from O₂ (Figure 6d).^[55] Spectroscopic structural characterization and DFT calculation provide strong evidence that the sp²-hybridized carbon near-ring ether defects along sheet edges are the most active sites for peroxide production. They proposed that the sp²-hybridized carbon near the epoxy (EP) group on an unannealed mrGO basal plane and the ring ether (ET) defects along the annealed mrGO sheet edges are the most active sites for H₂O₂ production. Smith et al. examined the H₂O₂ formation activities of the active sites proposed by McCloskey, and found that their catalytic activities were actually very low by means of first-principles calculations (Figure 6e).^[10] They systematically investigated the H₂O₂ formation activities

of different oxygen functional group structures on mrGO based on experimental observations. They discovered that two types of oxygen functional group structures (2EP and 1ET + 1EP) exhibited comparable or even lower overpotentials (<0.10 V) for H₂O₂ formation compared with the state-of-the-art PtHg₄ electrocatalyst. Their theoretical results reveal that the graphene edge and the synergistic effects between different oxygen functional groups are essential for the superior performance of mrGO for H₂O₂ production.

3.2.3. Nitrogen Types (Graphitic-N, Pyridinic-N, and Pyrrolic-N)

The nitrogen dopants in the carbon-based catalysts can significantly decrease the overpotential for the 2e⁻ ORR pathway, according to decreasing reaction Gibbs free-energy and optimizing the binding energy of *OOH, respectively.^[60] For instance, Fornasiero et al. reported a N-doped graphitized carbon nanohorns catalyst, which displayed high 2e⁻ ORR selectivity over a wide pH range (Figure 7a).^[40b] The authors attribute the high H₂O₂

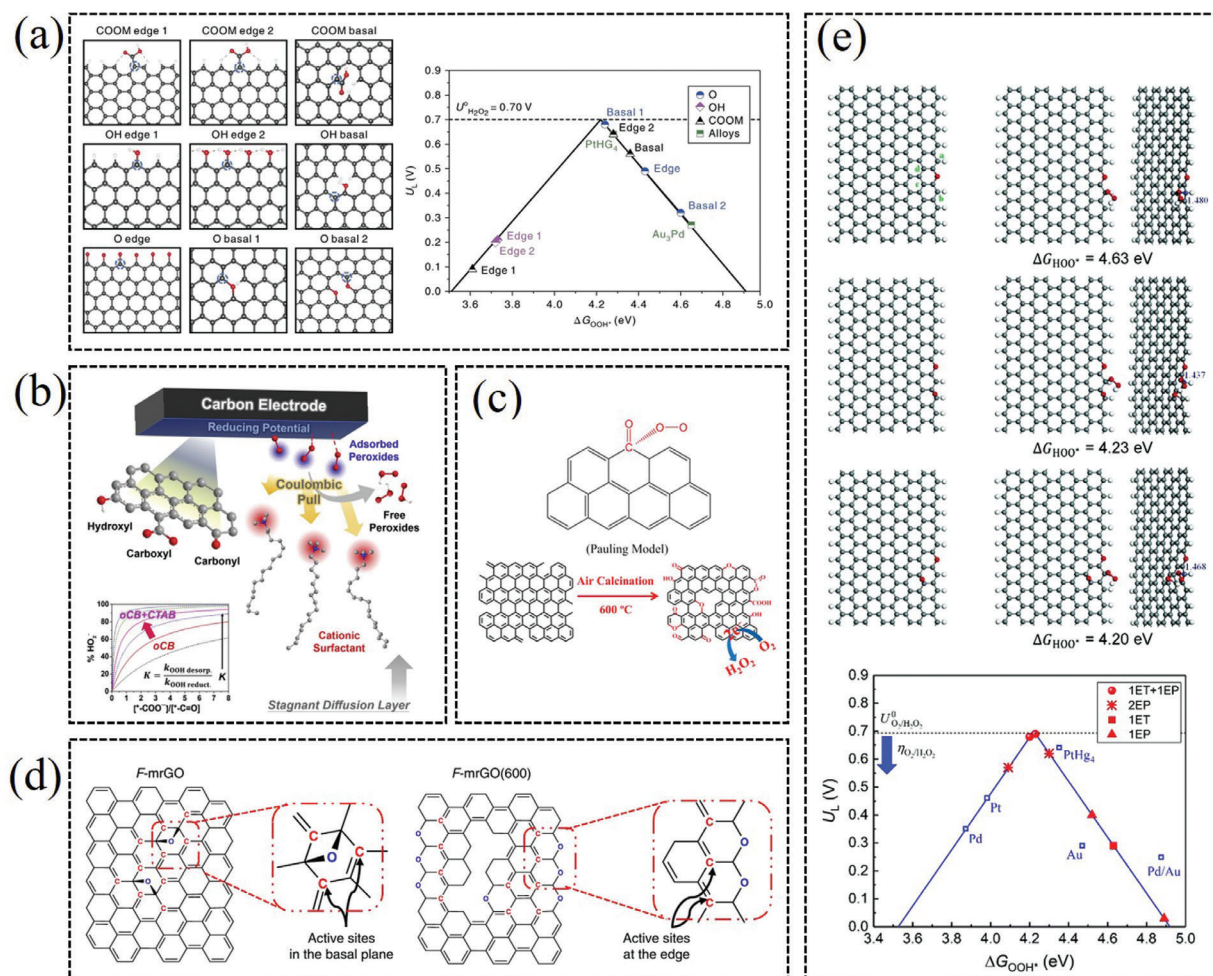


Figure 6. a) Oxidized carbon catalysts with various oxygen functional groups for $2e^-$ ORR. Reproduced with permission.^[15a] Copyright 2018, Springer Nature. b) In situ engineering of carbon catalyst with surface COO^- groups as main active sites and surface $C=O$ groups for H_2O_2 selectivity. Reproduced with permission.^[59] Copyright 2020, Elsevier. c) Carbon black oxidized by air calcination for enhanced H_2O_2 generation. Reproduced with permission.^[33b] Copyright 2019, American Chemical Society. d) Reduced graphene oxide catalyst with sp^2 -hybridized carbon near-ring ether defects or sheet edges as active sites for H_2O_2 production. Reproduced with permission.^[55] Copyright 2018, Springer Nature. e) Mildly reduced graphene oxide catalyst with two types of oxygen functional group structures (2EP and 1ET + 1EP) as active sites for $2e^-$ ORR. Reproduced with permission.^[10] Copyright 2019, Royal Society of Chemistry.

selectivity under acidic conditions to the effective protonation of the pyridine-N, which reduces the catalytic center's ability to break the O–O bond. Wu et al. studied the microscopic relationship between the bonding configuration of various nitrogen-doped graphene and the reactivity/mechanistic process toward H_2O_2 production via DFT calculation method (Figure 7b).^[61] They propose that the catalytic reactivity of various sites follows this order: pyridinic-N graphene > pyrrolic-N graphene > graphitic-N graphene > pristine graphene. Except for the pyridinic-N, the graphitic-N maybe is also feasible to H_2O_2 electroproduction via $2e^-$ ORR.^[62] For instance, Sidik et al. investigated the effect of graphite-N sites in Ketjenblack to $2e^-$ ORR catalytic performance by an experimental and theoretical study. The quantum calculations demonstrate that the carbon radical sites formed adjacent to the graphite-N are active for oxygen electroreduction to H_2O_2 (Figure 7c).^[63] Strasser et al. explored the $2e^-$ ORR electrocatalytic performance of a number

of nitrogen-doped mesoporous carbon catalysts, which achieved H_2O_2 selectivity of 95–98% in acidic solution (Figure 7d).^[39b] Nitrogen doping was found to sharply boost H_2O_2 activity and selectivity. Until now, most studies consent the pyridinic-N and graphitic-N are electroactive for H_2O_2 generation by adjusting the electronic structure of adjacent carbon sites, which is instructive for designing high efficiency $2e^-$ ORR nitrogen-doped catalysts.

3.2.4. Synergistic Effect

The synergetic effect between different functional groups and other catalytic active moieties is also crucial to adjust the catalytic activity of catalysts for H_2O_2 generation. Many catalysts generally consist of various active sites to maximally boosting their catalytic performance.^[64] For instance, Bao et al. reported a boron and nitride co-doped carbon catalyst for efficiently

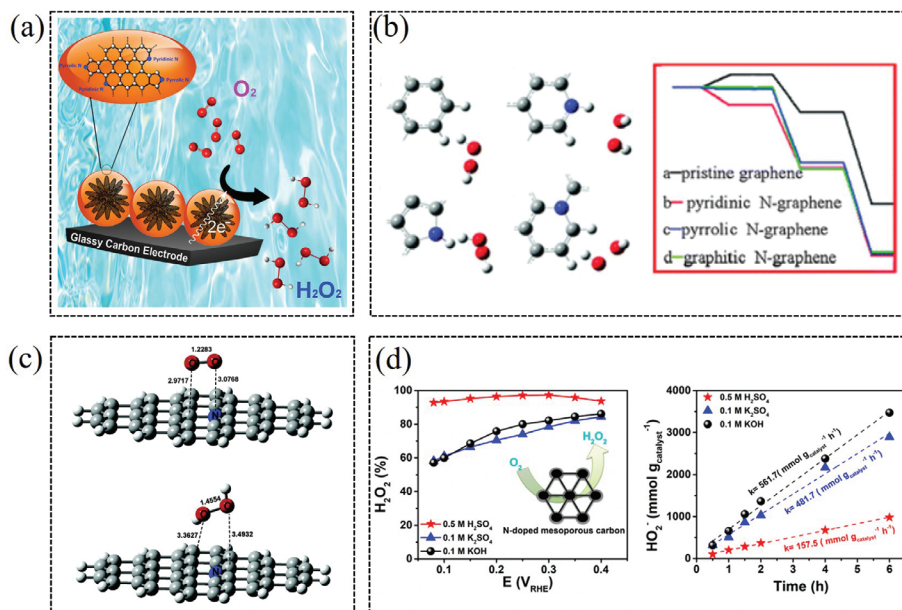


Figure 7. a) N-doped graphitized carbon catalyst for highly production of H_2O_2 . Reproduced with permission.^[40b] Copyright 2018, Elsevier. b) H_2O_2 production reactivity of nitrogen-doped graphene within various carbon lattices. Reproduced with permission.^[61] Copyright 2013, Royal Society of Chemistry. c) $2e^-$ ORR catalytic performance of nitrogen-doped graphite with graphite-N as actives. Reproduced with permission.^[63] Copyright 2006, American Chemical Society. d) Nitrogen-doped mesoporous carbon catalysts for H_2O_2 production. Reproduced with permission.^[39b] Copyright 2018, American Chemical Society.

electrochemical synthesis of H_2O_2 (Figure 8a).^[40a] The *h*-BN domains in graphitic structures provide higher activity and selectivity for the $2e^-$ ORR process in comparison to individual B or N doped structures. Furthermore, experimental and DFT results illustrate that the interface between *h*-BN domains and graphene exhibits unique catalytic behavior and can preferentially drive the production of H_2O_2 . Zhang and co-workers reported that the Co– N_x –C sites and oxygen functional groups, including C–O and –COOH species, contributed to the reactivity and selectivity for H_2O_2 electrogeneration, respectively (Figure 8b).^[65] The experimental results show that only atomic Co– N_x –C sites can afford ideal ORR reactivity but poor selectivity for $2e^-$ ORR, while only abundant oxygen functional groups can provide high H_2O_2 selectivity and inferior ORR reactivity. Zhao et al. constructed a COOH-terminated nitrogen-doped carbon aerogel electrocatalyst, which exhibited a complete 100% selectivity to H_2O_2 with high yields and stability (Figure 8c).^[46] Both theoretical and experimental results indicate the real role of the N heteroatom coexisting with COOH groups in boosting the activation of oxygen for the $2e^-$ ORR. With the development of uncovering the catalytic active sites of catalysts, designing the catalysts with synergistic effect active sites maybe is potential strategy for high efficiency $2e^-$ ORR catalysts.

3.2.5. Others (pH, Applied Potential, Pore Structure, and Steric Hindrance Effect)

For various $2e^-$ ORR catalysts, the pH environment also has an effect on the activity and selectivity for H_2O_2 production.^[39b,43,51,52,66] As shown in Figure 9a, Noffke et al.

proposed a catalytic model based on interfacial solvation and dielectric constant to understand pH-dependent selectivity for ORR.^[66] The synthesized N-doped graphitic carbon catalyst displays the two-electron ORR pathway in acid medium, while exhibits $4e^-$ ORR process in alkaline electrolyte. Iglesias et al. performed rotating ring disk electrode experiments under various pH conditions in order to confirm the selectivity of the catalytic process.^[40b] The results show that the lower pH with a higher proton concentration mainly leads to $2e^-$ reaction to H_2O_2 , while the higher number of electrons of catalyst at alkaline pH is less selective toward H_2O_2 production. In addition, various studies demonstrate that both H_2O_2 selectivity trend and the number of transferred electrons are associated with the applied potential.^[51,67] For instance, Xiao et al. investigated the influence of applied potential to the ORR selectivity using reduced graphene oxide aerogels catalysts. The effect of the applied potential on the ORR selectivity can be understood from the following two aspects. On one hand, the applied potential acts as a driving force for the catalytic reaction, which inevitably affects the reaction process. On the other hand, the adsorption of some spectator species (OH_{ad}) are also affected by the applied potential, which in turn also affects the target reaction.^[67]

The porous structures, including pore size and porosity, are crucial factors for catalytic performance of $2e^-$ ORR, mainly influencing the mass transport process in catalyst layer.^[14b,44] The presence of regular micropores may decrease the residence time of the H_2O_2 on the electrochemical catalysts, thus contributing to prevent further reduction of H_2O_2 to water. Park et al. prepared a series of mesoporous nitrogen-doped carbon catalysts, exhibiting well-ordered mesopores with diameters of 3.4–4.0 nm, which displayed high selectivity toward H_2O_2 over 90% (Figure 9b).^[44]

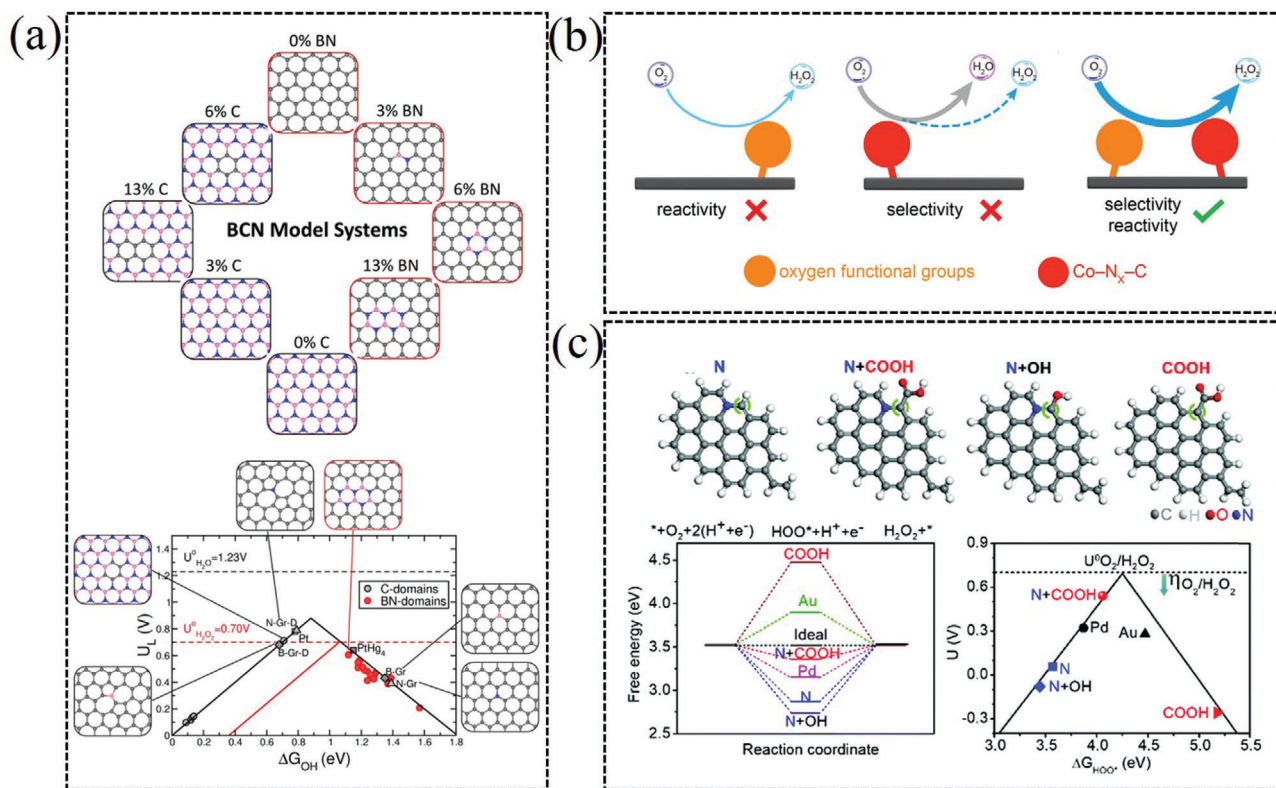


Figure 8. a) Designing boron nitride islands in carbon catalyst for efficient $2e^-$ ORR. Reproduced with permission.^[40a] Copyright 2018, American Chemical Society. b) Electrosynthesis of H_2O_2 synergistically catalyzed by atomic $Co-N_x-C$ sites and oxygen functional groups. Reproduced with permission.^[65] Copyright 2019, Wiley-VCH. c) A COOH-terminated nitrogen-doped carbon aerogel as electrochemical catalyst for H_2O_2 generation. Reproduced with permission.^[46] Copyright 2019, Royal Society of Chemistry.

Such high selectivity toward H_2O_2 is probably due to good mass transport of the mesoporous structure and abundant exposed active sites in the catalyst layer. Xiao et al. reported rGO/PEI aerogel catalyst with enhanced H_2O_2 electrogeneration selectivity, which was related to the steric hindrance effect (Figure 9c).^[67] The 3D porous structure of aerogels and the steric hindrance effect between PEI and rGO interface endow enhanced $2e^-$ catalytic selectivity (90.7%), production rate ($106.4 \text{ mmol g}_{\text{catalyst}}^{-1} \text{ h}^{-1}$) and durability for H_2O_2 electrogeneration.

3.3. Non-Noble Transition Metal Catalysts

Non-noble transition metal catalysts, such as transition metal oxide (TMO) and metal–nitrogen modified carbon ($M-N-C$, $M = Mn, Fe, Co, Ni, Cu, \text{etc.}$), are widely studied for electrocatalytic production of H_2O_2 , due to their low cost and environmental compatibility. Nevertheless, the pristine TMO generally exhibits limited catalytic activities and insufficient durability, probably because of their intrinsic electronic structure, low conductivity, unideal mass transfer, and agglomeration. Loading metal oxides on conductive carbon supports is a promising strategy to overcome these limitations. For instance, using Vulcan XC 72 as carbon support, a series of TMO/C catalysts, such as CeO_2/C ,^[68] $SnNi/C$,^[69] TiO_2-Au/C ,^[70] V/C ,^[71] ceria/C,^[72] and MnO_2/C ,^[58c] are investigated for the reduction of O_2 to H_2O_2

with the high activity and selectivity. Printex L6 is another commercial carbon support to construct TMO/C catalysts for electrogeneration of H_2O_2 , such as CeO_2/C ^[68b] and ZrO_2/C .^[73] Additionally, some graphene supported metal oxide catalysts, such as $\gamma-Fe_2O_3@graphene$,^[74] ZrO_2-rGO ,^[75] and $MnCO_3/GO$ ^[76] catalysts show high selectivity toward $2e^-$ ORR to H_2O_2 electrogeneration. Recently, some Zn and Co activated carbon catalysts were also used for electrogeneration of H_2O_2 via $2e^-$ ORR.^[77] The catalytic performances of some carbon-based catalysts are listed in Table 2. These studies show that lower quantities of metal on carbon supports are more active for H_2O_2 formation.

Recently, the specific transition metals are introduced into nitrogen-doped carbon frameworks with forming metal–nitrogen ($M-N_x$) moieties to stabilize and activate metal cations.^[16,65] The $M-N_x$ moieties generally are contributed to the high catalytic performance for $2e^-$ ORR. For instance, Strasser et al. combined computational and experimental efforts to uncover the trends in electrochemical H_2O_2 production over a series of $M-N-C$ materials (Figure 10a).^[16] The $Co-N-C$ catalyst is uncovered with outstanding H_2O_2 productivity high selectivity (80%) in 0.5 M H_2SO_4 . Additionally, porous manganese and nitrogen co-doped carbon nanorods could catalyze reduction of oxygen in an acidic environment with >98% H_2O_2 selectivity (Figure 10b).^[78] Chio et al. investigated the active sites in $Fe-N-C$ catalysts toward H_2O_2 production, which demonstrated that both FeN_xC_y moieties and Fe particles encapsulated in

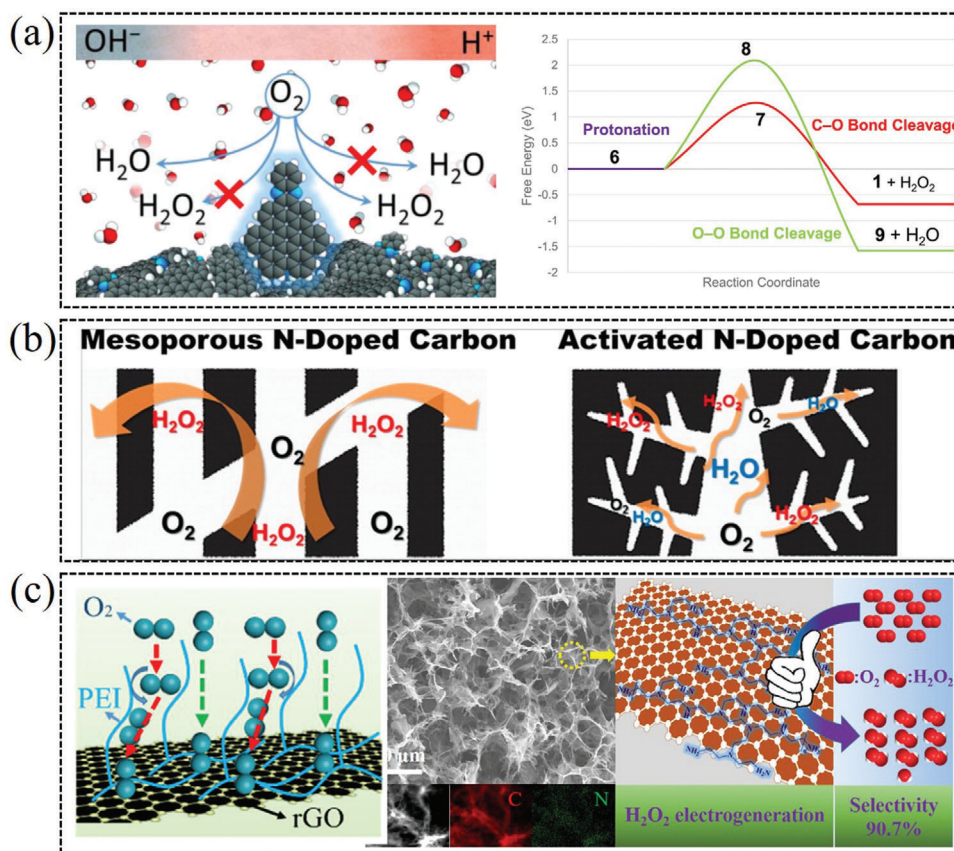


Figure 9. a) A model for the pH-dependent selectivity of the ORR electro-catalyzed by N-doped graphitic carbon. Reproduced with permission.^[66] Copyright 2016, American Chemical Society. b) Mesoporous nitrogen-doped carbon with highly selective 2e⁻ ORR performance than microporous catalyst. Reproduced with permission.^[44] Copyright 2014, American Chemical Society. c) Steric hindrance effect on PEI/rGO interfaces and the selectivity of H₂O₂ electrogeneration. Reproduced with permission.^[67] Copyright 2018, American Chemical Society.

N-doped carbon layers exhibited moderately catalytic activity toward 2e⁻ ORR (Figure 10c).^[79] Li et al. reported Co-N_x-C and oxygen functional group co-modified carbon electrocatalyst exhibited excellent catalytic performance for H₂O₂ generation, corresponding to a high selectivity over 80% in 0.10 M KOH (Figure 10d).^[65] For the non-noble transition metal catalysts, optimizing the transition metal sites and functional carbon supports are essential to regulate their catalytic active sites, conductivity and mass transfer process, which can further improve the 2e⁻ ORR catalytic performance.

3.4. Single-Atom Catalysts

In recent years, single-atom catalysts (SACs) have received increasingly attentions for their particularly high activity and selectivity to produce H₂O₂ via 2e⁻ ORR pathway. One of the significant advantages of SACs is that it could offer near 100% utilization of metal atoms as active sites. More importantly, the underlying substrate can dramatically modify the electronic structure of supported single-atom, thus altering the activity and selectivity of the active sites.^[17,28,86] Therefore, extensive investigations have been devoted into single-atom catalysts to examine

the possible structure–property correlation regarding activity and selectivity of single-atom catalysts for H₂O₂ production.

As a sample, Lee and co-workers predicted that Pt single-atoms could be stabilized on N-vacancy sites of titanium nitride support by the DFT calculations, and prepared Pt/TiN single-atom catalyst with the high selectivity toward H₂O₂ (65%) generation.^[87] Unlike Pt nanoparticles, the Pt single-atom catalyst can predominantly produce hydrogen peroxide in the electrochemical oxygen reduction with the highest mass activity reported so far (Figure 11a).^[28] Tremendous efforts have done to comprehensively understand the underlying high selectivity/activity of single-atom catalysts toward H₂O₂ production. Huang et al. simultaneously screened out seven single-atom catalysts with higher activity and selectivity toward H₂O₂ production than the PtHg₄ in acidic media by means of large-scale DFT computations (Figure 11b).^[12] This machine-learning method is very helpful for establishing the intrinsic structure–property correlations and accelerating the discovery of more efficient single-atom catalysts via two-electron ORR. Fe-CNT SACs presents the maximum H₂O₂ selectivity of more than 95% in both alkaline and neutral electrolyte. The catalytic C and Fe active sites in Fe⁻C–O moieties are responsible for the H₂O₂ generation pathways by the DFT calculation (Figure 11c).^[88] Recently, Liu et al. systematically studied that the relation between the structure of transition metal (Mn, Fe, Co,

Table 2. The electrochemical performance of some non-noble transition catalysts.

Electrocatalysts	Electrolytes	H ₂ O ₂ (%)	E _{onset} vs RHE	N	Reference
Nb ₂ O ₅ -rGO	0.1 M K ₂ SO ₄ /0.1 M NaOH	85.374.9	0.3 V/0.7 V	≈2.32.5	[80]
Co _x O _y /C	1 M NaOH	74	≈0.85 V	2.4	[81]
4% CeO ₂ /C	1 M NaOH	88	≈0.75 V	≈2.2	[68a]
CeO ₂ /C	1 M NaOH	44	≈0.75 V	3.1	[68b]
SnNi/C	1 M NaOH	88	≈0.7 V	≈2.2	[69]
CoS ₂	0.05 M H ₂ SO ₄	≈70	≈0.7 V	2.6	[82]
Co-NC	0.1 M H ₂ SO ₄	≈100	≈0.75 V	–	[83]
Fe ₃ O ₄ /PrintexFe ₃ O ₄ /graphene	1 M KOH	6862	≈0.6 V	≈2.6≈2.8	[84]
Co-C	0.1 M HClO ₄	80±5	≈6.2 V	2.4	[77d]
Co-N-C	0.5 M H ₂ SO ₄	80	≈0.78 V	2.4	[16]
Oxidized Co-N-C	0.1 M HClO ₄	> 85	–	–	[85]
Mn-N-C	0.1 M HClO ₄	> 98	≈0.7 V	≈2.0	[78]
Co-POC	0.1 M KOH	80	0.79 V	2.4	[65]

Ni, and Cu) single-atom catalysts anchored in nitrogen-doped graphene and the catalytic performance for H₂O₂ synthesis. The results show that the Co single-atom exhibits optimal d-band center and can be operated as a highly active/selective catalyst for H₂O₂ synthesis (Figure 11d).^[17] In addition, Zhang et al. reported a hierarchical free-standing single-Co-atom (with Co-N₄ coordination) electrode to efficiently produce H₂O₂ via a 2e⁻ ORR pathway in acidic media.^[89] For the single-atom 2e⁻ ORR catalysts, more work should be focused on improving the loading of single-atoms and compatibility for various acid/alkaline/neutral electrolyte, which is vital for constructing membrane electrode assembly (MEA) and practical application. Some advanced technologies, such as machine-learning method, characterization technique (electron microscope/synchrotron radiation) and DFT calculation, maybe are helpful to recognize the structure and catalytic active sites of the catalysts.

3.5. Molecular Complexes

Molecular complexes, including metal molecular complexes and nonmetal organic molecular complexes, are also widely investigated as heterogeneous two-electron ORR catalysts in aqueous solutions at various pH values. Generally, the metal molecular complexes are composed of transition metal ion centers (mainly 3d transition metals, such as Fe, Co, Cu, Mn, and Ni) and organic macrocycles ligands (porphyrin, pyrazine, quinones and viologens-type derivatives).^[90] Recently, various reports demonstrate that the nonmetal organic molecular complexes and noble-metal molecular complexes also exhibit two-electron ORR catalytic performance.

The species of metal molecular complexes for 2e⁻ ORR catalysts mainly include iron, cobalt, and manganese complexes. In 1979, Bettelheim and Kuwana reported that the water soluble iron(III) tetra-(4-N-methylpyridyl)porphyrin pentachloride (Fe^{III}T4MPyP) could catalyze the electrochemical reduction of oxygen with an ultrahigh H₂O₂ yield of 95%.^[91] Thereafter, a series of Fe-based molecular complexes are studied as 2e⁻ ORR catalysts, such as modification of ligands (Fe^{III}TPPS)^[92] and

synthetic metal centers (Cu(TPA) linked to iron porphyrin).^[93] Notably, cobalt molecular complexes, such as Co-porphyrins, Co-phthalocyanines, and Co-macrobicyclic hexamine, generally exhibit desirable 2e⁻ electrochemical activity for producing H₂O₂.^[94] Smith et al. reported a cobalt tetraphenylporphyrin (Co-TPP) supramolecular for direct electrosynthesis of H₂O₂ in neutral water. Site isolation of Co-TPP active sites within a porous organic cage architecture enables high H₂O₂ selectivity (90–100%) and productivity (Figure 12a).^[95] Additionally, some cobalt porphyrin polymers, such as pCoTAPP and Co(TCPP), are found to be efficient photo-electrocatalysts for the photosynthesis of hydrogen peroxide via a 2e⁻ ORR pathway.^[94b,96] Extensive researches have been explored on the mechanism and activity of molecular Schiff base cobalt compounds for the selective electrocatalytic reduction of O₂ to H₂O₂.^[97] For instance, S. Stahl reported one N₂O₂-ligated cobalt complex catalyst using decamethylferrocene (Fc⁺) as the reductant and acetic acid as the proton source, which exhibited high selectivity toward H₂O₂ electroproduction (93–99%) (Figure 12b).^[98] With a similar catalytic mechanism of cobalt molecular derivatives, the Mn-based molecular complexes, containing either porphyrins or porphyrin derivatives, can be also applied to electrocatalytically reduce O₂ under aqueous conditions.^[99] Machan et al. reported a molecular manganese (III) complex, with a bipyridine-containing Schiff base-type ligand (Mn(^{tbu}dcbpy)Cl), which is active for the electrocatalytic reduction of O₂ to H₂O₂ with above 80% Faradaic efficiency. Mechanistic studies demonstrate that the catalytically active species have been generated through the interaction of the added proton donor and the parent Mn complex (Figure 12c). Stopped-flow spectrochemical results demonstrate that the catalyst produces H₂O₂ by an proposed ECCEC (the abbreviation of reaction paths) mechanism, and less-than-quantitative selectivity is attributed to a thermal disproportionation reaction of H₂O₂.^[100]

Besides the metal molecular complexes mentioned above, some metal-free organic molecules have also shown catalytic activity for the two-electron ORR. Yin et al. reported a heterogeneous organic molecular electrocatalyst, 2, 2'-dipyridylamine, with a high H₂O₂ catalytic activity (onset potential of ≈0.60 V

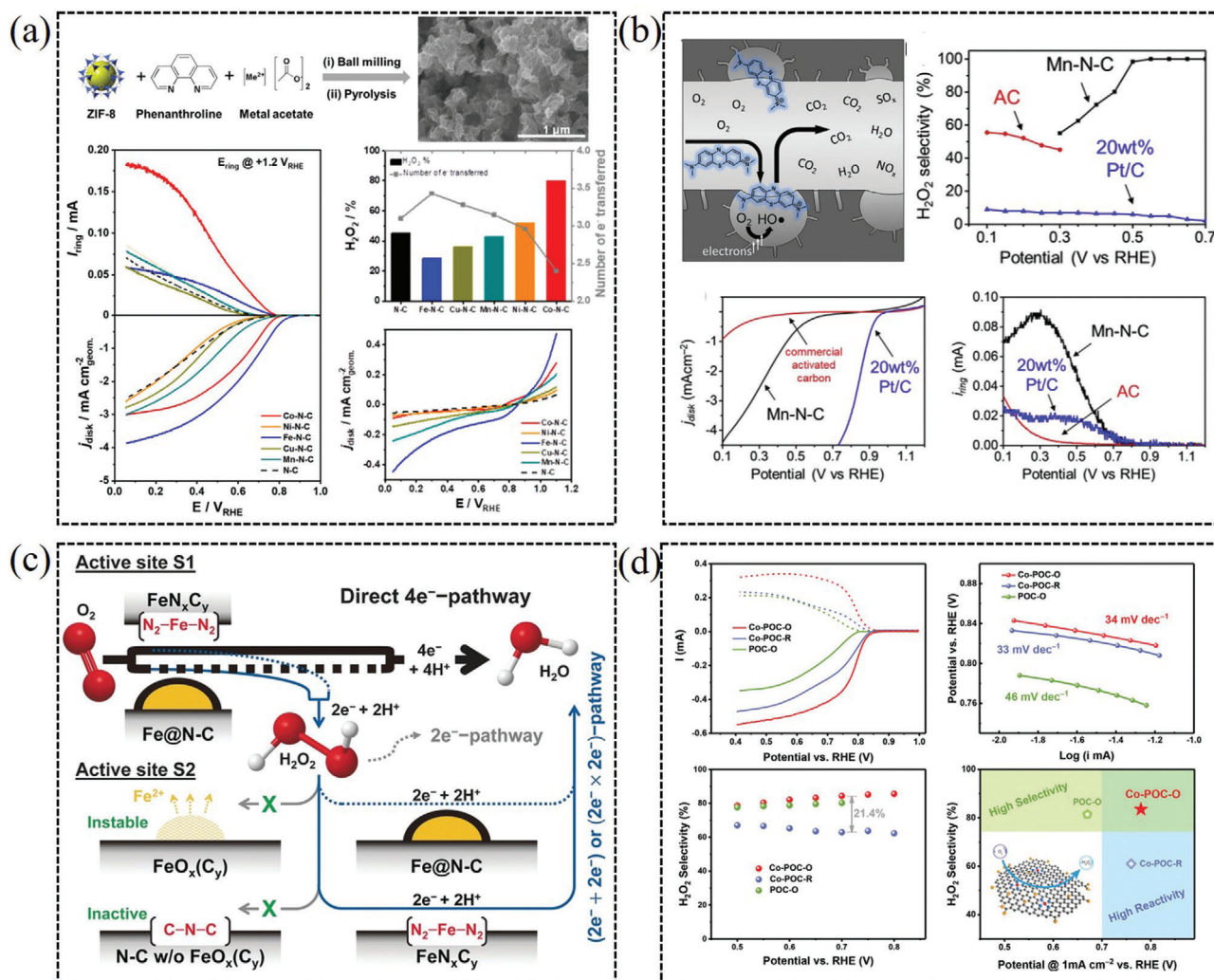


Figure 10. a) M–N–C catalysts on the catalytic activity and selectivity for hydrogen peroxide production. Reproduced with permission.^[16] Copyright 2019, American Chemical Society. b) Efficient H₂O₂ generation in highly porous manganese and nitrogen co-doped carbon nanorods. Reproduced with permission.^[78] Copyright 2019, Elsevier. c) Investigation of the nature of active sites toward ORR in Fe–N–C catalysts. Reproduced with permission.^[79] Copyright 2017, Wiley-VCH. d) Production of H₂O₂ synergistically catalyzed by atomic Co–N_x–C sites and oxygen functional groups. Reproduced with permission.^[65] Copyright 2019, Wiley-VCH.

vs RHE) and selectivity ($\approx 80\%$) in acidic aqueous electrolyte. In addition, the DFT study reveals a possible $2e^-$ ORR mechanism, in which the pyridyl- and amino-N play as the anchoring sites for reaction intermediates (Figure 12d).^[53] Mitra et al. reported that the conducting polymer PEDOT (poly(3,4-ethylenedioxythiophene)) was an efficient catalyst for the reduction of O₂ to H₂O₂ with Faraday efficiency close to 100%.^[101] Warczak et al. reported N,N'-dimethyl perylene-tetracarboxylic diimide (PTCDI) as an organic semiconductor catalyst for electrochemical generation of H₂O₂ in a pH range of 1–13, with a catalytic figure of merit up to 26 kg H₂O₂ per gram catalyst per hour.^[102] Peng et al. reported a 2D redox-active cationic covalent triazine network as an electrocatalyst for generating H₂O₂, which exhibited high catalytic selectivity ($\approx 85\%$) in a wide range of potentials (0.1–0.7 V vs RHE).^[103]

4. Application of Electrogenerated H₂O₂ via $2e^-$ ORR

Hydrogen peroxide, as an important chemical, is widely used as an oxidant and disinfectant in human society. Considering the disadvantages of traditional anthraquinone oxidation–reduction and Huron–Dow methods to produce H₂O₂ (dilute alkaline H₂O₂ solution), electrochemical oxygen reduction method to produce H₂O₂ recently gained tremendous attention, which can be used in various fields. It is necessary that H₂O₂ could be synthesized in small amounts directly at the place of need and at the right point in time. Electrochemical synthesis is the most common alternative method for production of H₂O₂ via the $2e^-$ ORR.^[38a,68a] This reaction makes the in situ H₂O₂ production from renewable power sources possible, and the scalability of electrochemical devices enables local and on-demand H₂O₂ production, which can

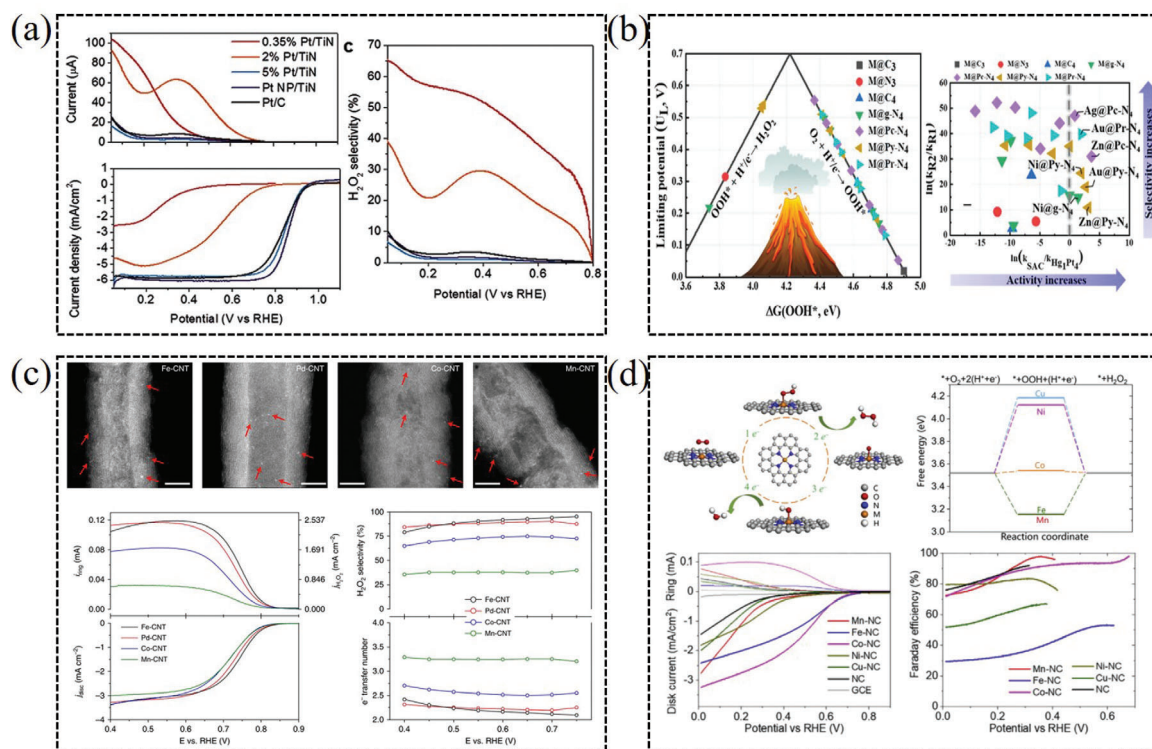


Figure 11. a) Single-atomic platinum supported on TiN for selective $2e^-$ ORR. Reproduced with permission.^[28] Copyright 2015, Wiley-VCH. b) DFT computations for representative experimentally achievable SACs toward $2e^-$ ORR. Reproduced with permission.^[12] Copyright 2019, American Chemical Society. c) Single-atom Fe-C-O as an efficient H_2O_2 catalyst. Reproduced with permission.^[88] Copyright 2019, Springer Nature. d) Atomically dispersed cobalt anchored in nitrogen-doped carbon as high efficiency electrocatalyst for H_2O_2 synthesis. Reproduced with permission.^[17] Copyright 2020, Elsevier.

reduce the costs associated with storage and transportation.^[104] This electrochemical H_2O_2 production method has potential application in many fields, such as organic pollutants degradation, water treatment, bacteria killing and disinfection, and energy storage.

4.1. Organic Pollutants Degradation

Industrial wastewater often contains many toxic organic pollutants, such as organic dyes, organic drug and other harmful organic molecular, which can pose a considerable threat to human health and potential long-term adverse effects on ecosystem.^[105] The Fenton method, based on the reaction between ferrous iron (Fe^{2+}) and hydrogen peroxide (H_2O_2) to produce hydroxyl radicals ($\cdot OH$), has been widely applied as advanced oxidation process. In the electro-Fenton process, the electrogenerated H_2O_2 can be effectively utilized as Fenton reagent to produce $\cdot OH$, which can be further used for the degradation of organic pollutants.^[106] The state-of-the-art electro-Fenton process is mainly worked in acid media, as the optimum pH for the Fenton reactions is in the range of 2.8–3.0. Therefore, it is an effective method to remove various organic pollutants in wastewater.

4.1.1. Organic Dyes

Amaranth is a typical representative of azo dyes. Producing H_2O_2 via $2e^-$ ORR under a neutral condition can be used

in Fenton reaction for removal amaranth,^[107] which processes high removal rate. In the same way, methyl orange,^[35b,108] methylene blue (Figure 13a),^[35a,78] acid blue 113 dye,^[109] acid orange,^[110] and rhodamine B^[33b,60] are also the common azo dye compounds existed in industrial wastewater. These dyes can be removed through the electrochemical reduction of O_2 to H_2O_2 and in situ generation of hydroxyl-free radicals. This method can efficiently degrade various organic pollutants and exhibit efficient total organic carbon removal in acidic or neutral condition.

4.1.2. Organic Drug

Some pharmaceutical compounds, such as antibiotic, trace pharmaceutical compounds, tetracaine, and ibuprofen are frequently detected in the aquatic environment, which can also pose a considerable threat to human health and ecosystem. Therefore, they are usually chosen as the target contaminant. Tetracycline as a common antibiotic can be degraded using in situ generation of H_2O_2 and radicals.^[108a,111] Trace pharmaceutical compounds, such as carbamazepine, cimetidine and amoxicillin, can be totally degraded within 1.5–3 h.^[108b] Ridruejo et al. reported that the generated H_2O_2 by CoS_2 -based catalyst in acidic medium could remove pharmaceutical tetracaine at 60–120 min by galvanostatic bulk electrolysis.^[112] As shown in Figure 13b, Ibuprofen can be also efficiently degraded by electro-Fenton process.^[113]

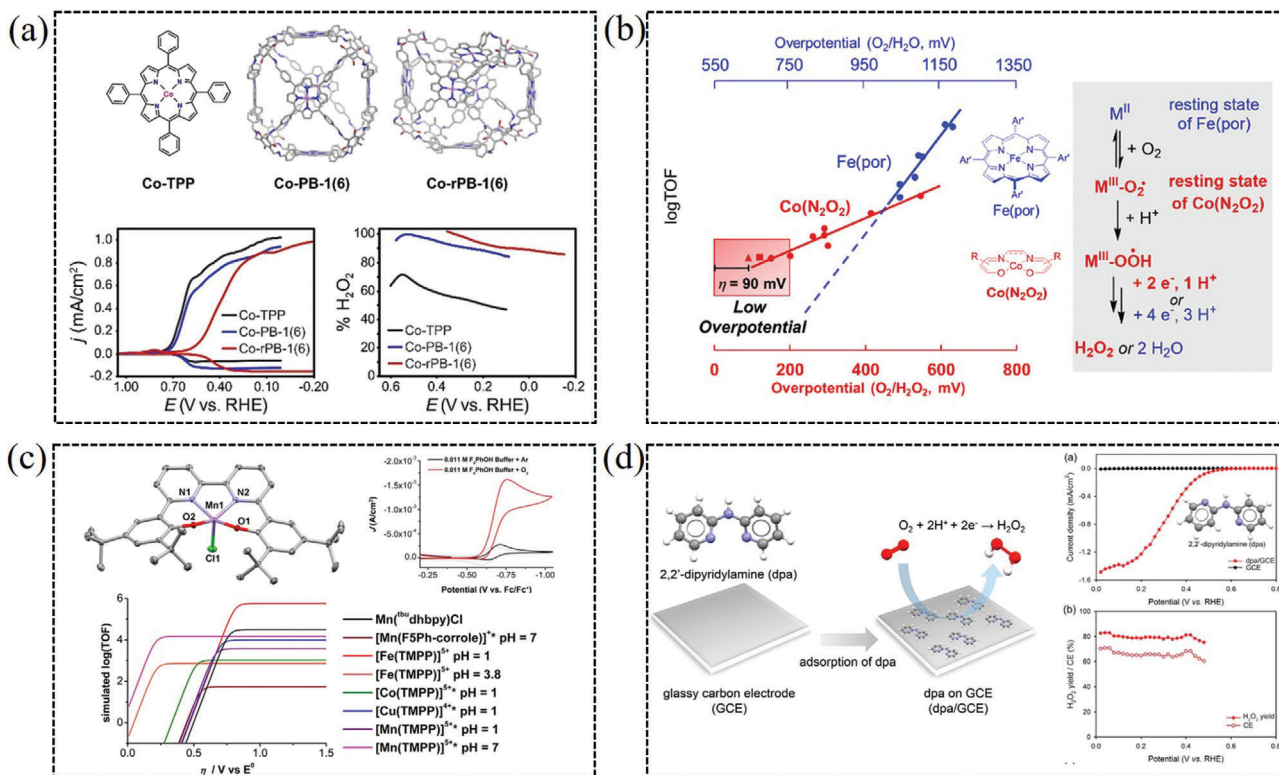


Figure 12. a) Supramolecular tuning enables selective electrocatalysis of H₂O₂ catalyzed by cobalt porphyrins. Reproduced with permission.^[95] Copyright 2020, Wiley-VCH. b) N₂O₂-ligated cobalt complexes for 2e⁻ ORR. Reproduced with permission.^[98] Copyright 2017, American Chemical Society. c) Molecular manganese complex with a bipyridine-containing Schiff base ligand for selective H₂O₂ production. Reproduced with permission.^[15b] Copyright 2018, American Chemical Society. d) 2,2'-dipyridylamine as heterogeneous organic molecular electrocatalyst for 2e⁻ ORR. Reproduced with permission.^[53] Copyright 2019, American Chemical Society.

4.1.3. Other Harmful Organic Molecules

Formaldehyde is harmful to the environment and human health. Therefore, treating industrial wastewater containing formaldehyde is of great importance. For instance, Wang et al. prepared a high-performance electrocatalyst from commercial CMK3 for in situ H₂O₂ production, which exhibited high performance for reducing formaldehyde in wastewater.^[32] The results show that the removal efficiency of formaldehyde (initial concentration of 14.0 mg L⁻¹) at different cell potentials are just for 30 min, corresponding to the highest efficiency at 2.7 V (up to 95%). Additionally, this method can markedly decrease the other harmful organics in wastewater, such as Phenol,^[35a] 4-chlorophenol,^[114] bisphenol A, dimethyl phthalate, and perfluorooctanoate, which are chosen as model contaminants due to their environmental persistence, bioaccumulation, and potential toxicity (Figure 13c).^[115] Those model contaminants can be efficiently removed through the heterogeneous electro-Fenton process for the selective two-electron ORR to intermediate H₂O₂, and the efficient total organic carbon removal can reach to 88–99% in short time.^[106] In addition, organophosphorus compounds, such as glyphosate and N (phosphonomethyl) glycine, have been extensively used as herbicide and classified as “probably carcinogenic in humans,” which are also efficiently degraded using the same methods.^[116] Therefore, in situ electrogeneration of H₂O₂ through 2e⁻ ORR represents

a potentially greener route for organic pollutants treatment in wastewater.

4.2. Water Treatment

The remarkable oxidation property of hydrogen peroxide allows it to oxidize various pollutants in waste water.^[117] Therefore, small-scale decentralized electrochemical production of H₂O₂ via a 2e⁻ ORR offers unique opportunity for sanitization applications and the purification of drinking water. For instance, Lian et al. report that the Fe₃O₄@GF (graphite felt) and in situ formed PGF (porous graphite felt) are attractive self-standing carbon materials for electrocatalysis of H₂O₂ and wastewater treatment, which simultaneously provide iron source toward electro-Fenton process for hydroxyl radicals (•OH) production. Furthermore, the degradation performance of PGF does not significantly decay even after 20 cycles of the repeated use, which provides the possibility to achieve swift water purification (Figure 14a).^[118] In addition, Li et al. reported that the in situ generated H₂O₂ in cathode combining with Fe²⁺ in anode could produce •OH via Fenton reaction to remove arsenite in solution, by efficiently oxidizing As(III) into As(V) and forming Fe(III)-As(V) precipitates, which is practically meaningful to apply in the degradation and removal of organic pollutants in water.^[119] As another example, Chen et al. reported that H₂O₂ synthesis using carbon catalysts in reaction bath could

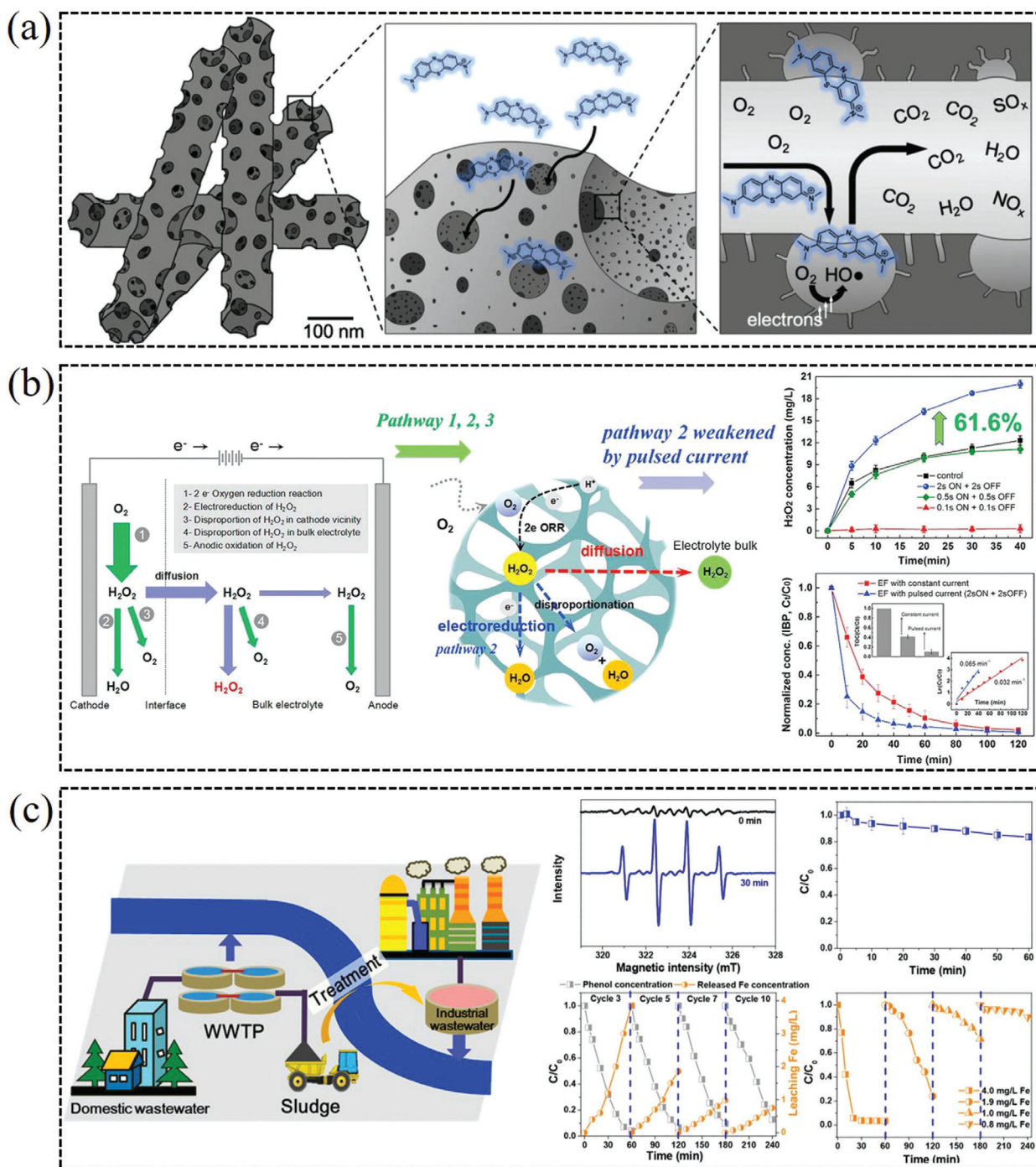


Figure 13. a) Organic dyes electrodegradation using porous manganese and nitrogen co-doped carbon nanorods catalyst via $2e^-$ ORR. Reproduced with permission.^[78] Copyright 2019, Elsevier. b) Drastic enhancement of H_2O_2 electrogeneration by pulsed current for ibuprofen degradation. Reproduced with permission.^[113a] Copyright 2018, Elsevier. c) Electrochemically catalytic degradation of phenol with H_2O_2 in situ generated and activated by a municipal sludge-derived catalyst. Reproduced with permission.^[115] Copyright 2018, American Chemical Society.

be directly applied in bleaching and the treatment of acidic waste streams (Figure 14b).^[41] Additionally, electrochemical synthesis of H_2O_2 in alkaline media is highly necessary. The alkaline H_2O_2 solution is widely used for bleaching and brightening in the pulp and paper industry as well as in many other areas.^[8a,77d]

4.3. Bacteria Killing and Disinfection

Hydrogen peroxide can be used in bacteria killing, which is one promising field in the delocalized or green-route water disinfection.^[120] Jiang et al. reported a low-cost Fe-CNT catalyst

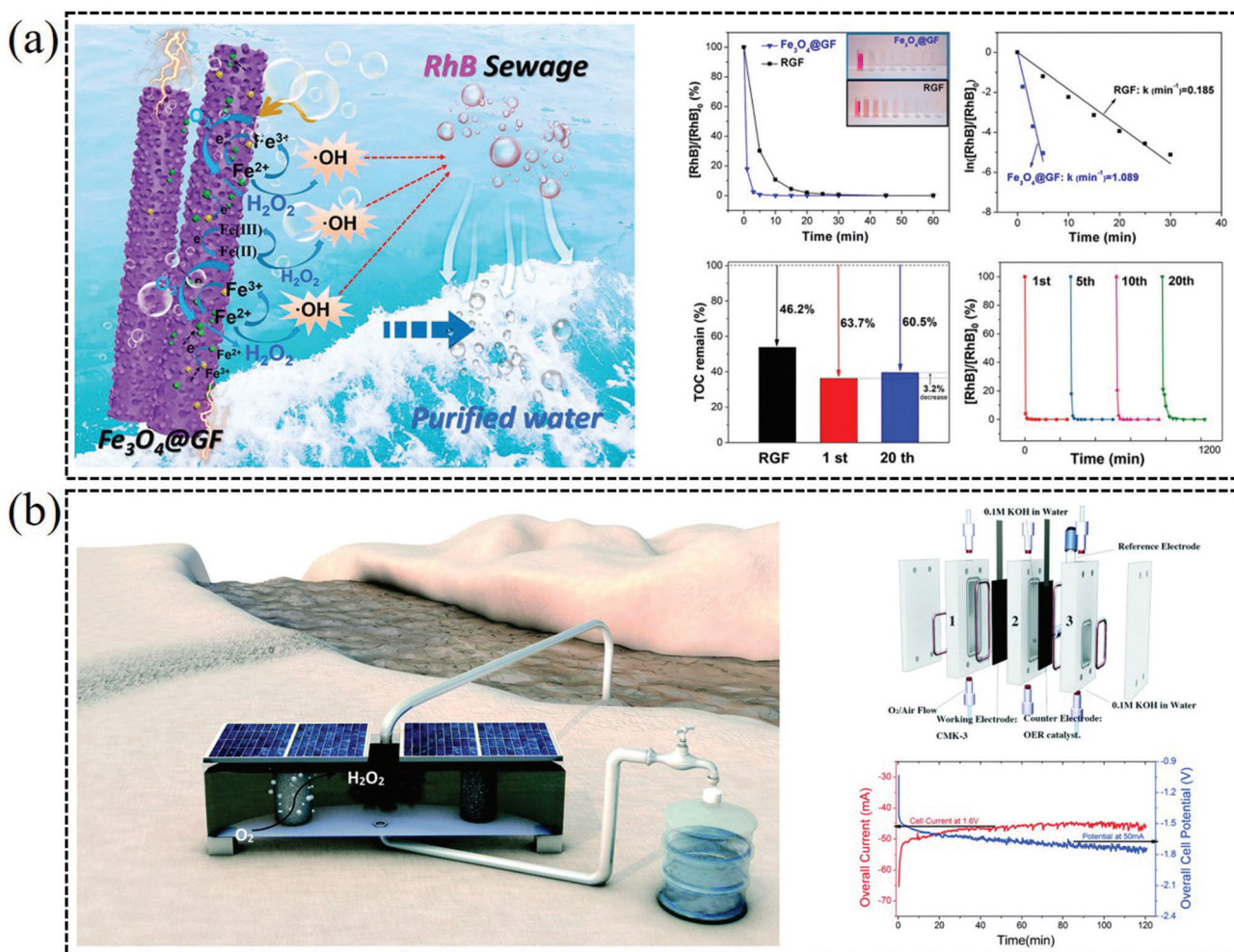


Figure 14. a) $\text{Fe}_3\text{O}_4@\text{GF}$ catalyst combined with electro-Fenton process for achieving swift water purification. Reproduced with permission.^[118] Copyright 2019, American Chemical Society. b) CMK-3 based carbon catalyst for electrochemical H_2O_2 generation and water purification. Reproduced with permission.^[41] Copyright 2017, Royal Society of Chemistry.

for highly efficient H_2O_2 generation and performed a prototype experiment to test the water disinfection effectiveness of the catalysts (Figure 15a).^[88] The results demonstrate that Fe-CNT has a rapid disinfection efficiency for *Escherichia coli*, delivering a 43% bacteria inactivation in 5 min and more than 99.9999% in 120 min with no recovery observed. In addition, Wang et al. reported $\text{GO}_x/\text{MnCO}_3$ catalyst can be used for in situ electrochemical synthesis of H_2O_2 via the $2e^-$ pathway, which can be onsite decomposed to form $\bullet\text{OH}$ radicals in neutral media to further kill bacteria.^[76] Therefore, in situ electrochemical synthesis of H_2O_2 via $2e^-$ ORR can provide an effective and environmentally friendly electrochemical approach for killing bacteria and disinfection applications.

4.4. Energy Storage

Hydrogen peroxide as an environmentally benign energy carrier can be produced by the electrocatalytic two-electron ORR (O_2 from abundant in air), which can be used to generate electricity through the setup of H_2O_2 fuel cells.^[121] Strasser et al. re-

ported a Co-N-C catalyst with high $2e^-$ catalytic performance during large-scale H_2O_2 production at high current densities in 0.1 M KOH (Figure 15b).^[16] When evaluated in a commercial microflow cell (MFC), the Co-N-C catalyst exhibits an unprecedented production rate of more than 4 mol peroxide $\text{g}_{\text{catalyst}}^{-1} \text{h}^{-1}$ at a current density of 50 mA cm^{-2} . Chen and co-workers demonstrated the cogeneration of electrical energy and H_2O_2 through a liquid Zn-air battery based on the oxygenated carbon black (Figure 15c), which could convert chemical energy into electrical energy for energy storage.^[122] In addition, hydrogen peroxide is also utilized as an alternative liquid oxidant in place of gaseous O_2 .^[121] Day et al. developed a successful photosynthetic process, focusing on the reduction of oxygen to H_2O_2 as a means of chemical energy storage, which could convert light energy into chemical energy for energy storage.^[96]

5. Summary and Outlook

H_2O_2 is a versatile and nontoxic commodity chemical, which is widely used in various fields. Electrochemical oxygen reduction via $2e^-$ pathway, instead of the industrial energy-intensive

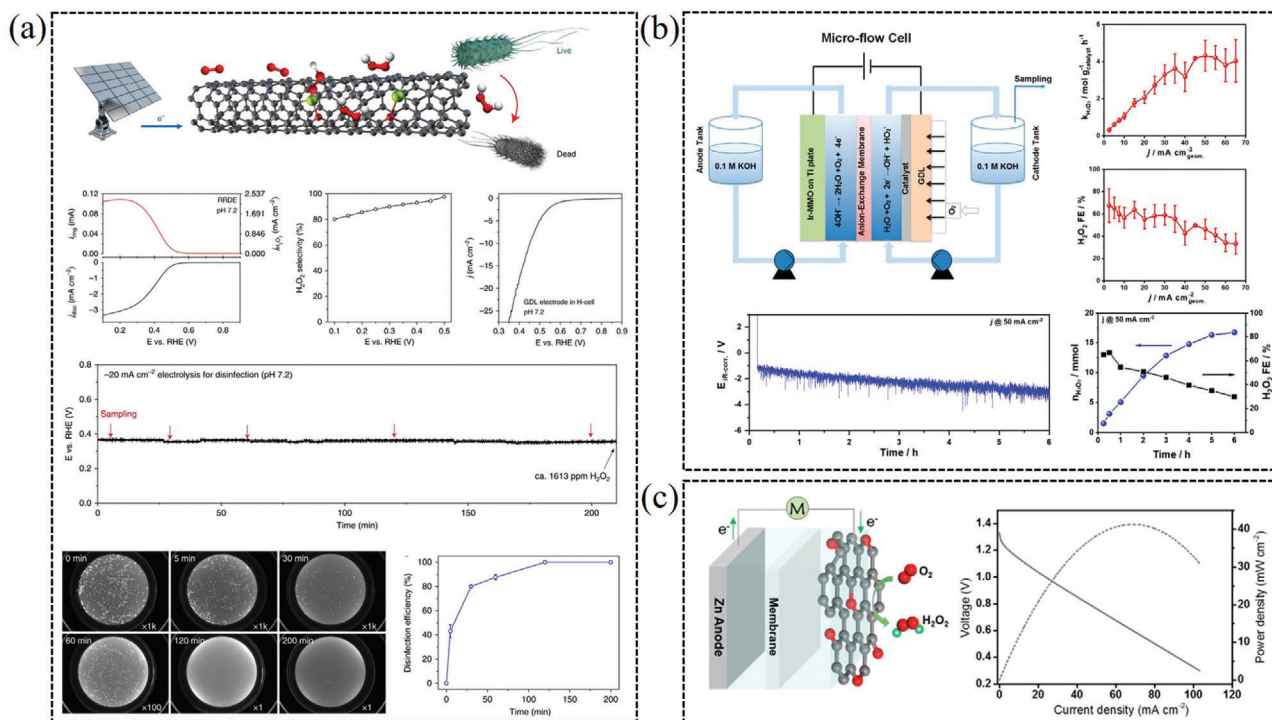


Figure 5. a) Fe-C-O as an efficient H₂O₂ catalyst for antibacteria and water disinfection. Reproduced with permission.^[88] Copyright 2019, Springer Nature. b) Microflow cell setup and H₂O₂ production rate at respective current densities on a Co-N-C electrode. Reproduced with permission.^[16] Copyright 2019, American Chemical Society. c) Oxygenated carbon electrocatalyst highly efficient production of electrical energy and H₂O₂ through a Zn-Air Battery. Reproduced with permission.^[122] Copyright 2018, American Chemical Society.

anthraquinone process and direct synthesis method, becomes increasingly important as an alternative/green method for H₂O₂ generation. Here, we summarized the development of 2e⁻ ORR electrochemical catalysts in recent years, in aspects of mechanism exploration, types of high-performance catalysts, factors to influence catalytic performance and potential applications. Until now, a diverse range of electrochemical catalysts are investigated for the electrochemical synthesis of H₂O₂, such as noble metal/alloys, carbon-based materials, non-noble transition metals, single-atom catalysts and molecular complexes. We have elucidated the factors that control the catalysis of electrochemical H₂O₂ production, such as electronic structure, carbon defect, functional groups (O, N, B, S, F etc.), synergistic effect, pH, pore structure, and steric hindrance effect. Additionally, the electrochemical synthesis of H₂O₂ exhibits attractive potential applications, containing wastewater treatment, organics degradation, disinfection, and energy storage.

Although intensive researches have been done in recent years, the grant challenges still exist for efficiently producing H₂O₂ via 2e⁻ ORR and exploring suitable in situ application of generated H₂O₂. Electrocatalyst is always the most critical factor to influence the generation efficiency of H₂O₂. The current 2e⁻ ORR catalysts generally exhibit lower catalytic efficiency, obscure catalytic sites, and inferior stability in various electrolytes. An ideal catalyst for two-electron ORR to produce H₂O₂ means that the adsorption of OOH* should be neither too strong nor too weak. And the selectivity of the catalysts is related to its ability to split the O-O bond. For the practical application, the 2e⁻ ORR catalysts also

should process the outstanding mass activity, conductivity and mass transfer performance. Additionally, the application of the electrochemical generation of H₂O₂ via 2e⁻ ORR can be deeply developed with various in situ devices, which is attractive in many scientific/industrial fields. In the further, more research maybe should be focused on the following aspects to further developing desirable 2e⁻ ORR electrocatalyst and promoting the wide application of 2e⁻ ORR.

i) Understanding mechanism of 2e⁻ ORR to H₂O₂

Exploring the catalytic mechanism is crucial and challenging for developing high efficiency 2e⁻ ORR catalysts. Some crucial technologies, including DFT calculation, high-throughput screening studies, machine learning method, and advanced characterization techniques (electron microscope/synchrotron radiation), can help us recognize the catalytic sites and catalytic mechanism. Among them, the DFT calculation is extremely useful for describe the key adsorption energies and reaction energy barriers. Nørskov et al. firstly developed the DFT calculation method using CHE model to describe the free energies of the intermediates and solvated protons/electrons on catalyst surface at a given potential. A common DFT calculation theme is based on that the 2D surfaces of catalysts (such as specific metal crystalline face, modified graphene, MN₄ moieties in graphene, ultrathin 2D metal oxides, boron nitride, etc.) interact with transition intermediates through oxygen atom. Generally, the well scaling relation between *OOH and *OH adsorption energies limits the 2e⁻ ORR

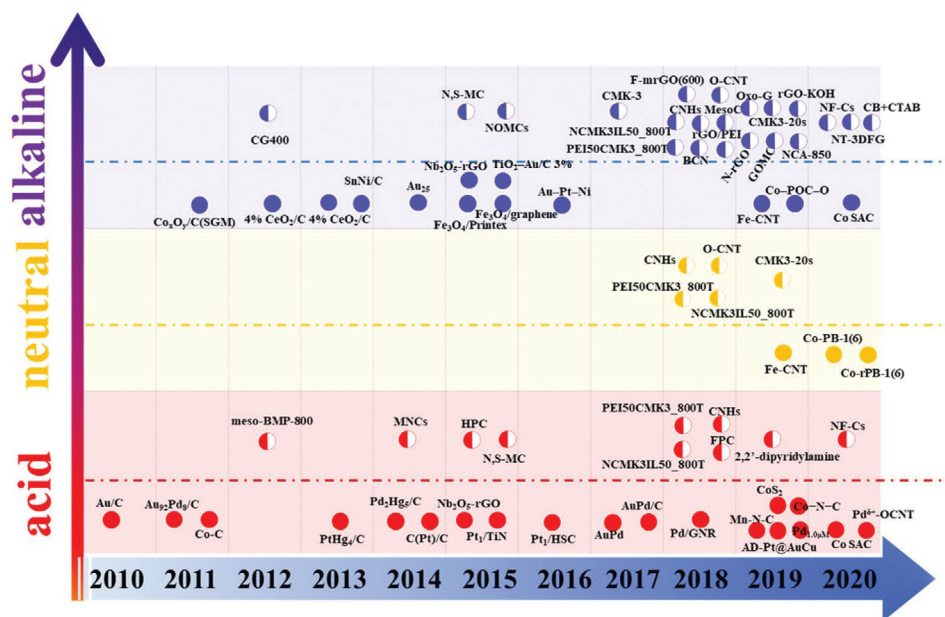


Figure 16. The diagram of summary some representative catalysts for H_2O_2 production through $2e^-$ oxygen electrochemistry in recent years (solid circle: metal catalyst; semisolid circle: nonmetal catalyst).

catalysts with both high catalytic activity and selectivity. To obtain $2e^-$ ORR catalysts with intrinsic high catalytic efficiency, we need to explore catalysts that break the scaling between $*OOH$ and $*OH$ adsorption energies. This will require active sites that bind $*OOH$ and $*OH$ differently. One possible strategy is introducing multifunctional active sites, which exhibit proper combination of binding sites. More factors should be considered in the further DFT calculation, including bifunctionality, interfacial sites, surface functionalization, confinement, electrolyte engineering etc. Some advanced DFT methods, such as post Hartree–Fock methods, cluster/DFT embedding schemes and hybrid functional, will be necessary to model those multifunctional catalysts in the future. Additionally, the high-throughput computational method is promising to discover new materials. The developing of advanced characterizations and analysis technologies, such as electron microscope/synchrotron radiation/nuclear magnetic resonance/machine learning method, are also vital to understand the catalytic sites and catalytic mechanism of $2e^-$ ORR.

ii) Factors that effect on achieving the desired ORR selectivity for H_2O_2

We have summarized the factors that influence the $2e^-$ ORR catalytic performance, including electronic structure, carbon defect, oxygen (N, B, etc.) functional groups, synergistic effect, pH, pore structure, and steric hindrance effect. Those factors are related to different catalytic active sites and further influence the catalytic performance. Through lots of catalytic mechanism are speculated, the universal relationships between the catalytic performance and structure of catalysts are still unclear. Meanwhile, insufficient understanding of which reaction steps are catalyzed by what sites, limits their progress. Therefore, more experimental and theoretical works are needed to elucidate the general re-

lationship between $2e^-$ catalytic performance and catalytic sites, catalysts' structure and the aforementioned factors.

The recent research tendency of some representative $2e^-$ ORR catalysts in acidic/alkaline/neutral electrolyte are summarized in **Figure 16**. It is noteworthy that most researches focus on the electrochemical generation of H_2O_2 in acidic and alkaline electrolyte, while the studies in neutral electrolyte are limited. In view of practical application, H_2O_2 produced in acidic medium can be usually used for oxidation purpose in organic synthesis, wastewater treatment or energy storage and conversion, and H_2O_2 generated in alkaline solution could be used for pulp and paper bleaching. Generally, the H_2O_2 produced in acidic and alkaline medium has limited practical application due the influence of pH. Thus, H_2O_2 produced in neutral aqueous should be studied intensively, which is thought to be the most useful and flexible form in their practical applications.

iii) The design of efficient catalysts

Plentiful catalysts have been studied for electrochemical generation H_2O_2 via $2e^-$ ORR pathway. For the practical application, the $2e^-$ ORR catalysts also should process outstanding catalytic activity/selectivity/stability, mass activity, conductivity, mass transfer performance and low cost. It still processes huge challenges to further develop high performance $2e^-$ ORR catalysts as follows.

Noble-metal/alloys catalysts process high catalytic efficiency, while the high price of catalyst hinders their large-scale application. More work should be done to optimize their mass loading/mass activity, and the compatibility in alkaline/neutral electrolyte in the future. Single-atom catalysts generally process proper catalytic selectivity and the highest atomic catalytic performance. However, the loading of single-atoms is generally low, and it still lacks an efficient route for synthesizing

single-atom catalysts with high yield and stability. Carbon based materials also display suitable $2e^-$ ORR catalytic performance and attractive application prospect, due to their high conductivity/stability, excellent porosity for mass transfer and low-cost. More works should focus on improving their catalytic efficiency and exploring the catalytic sites/mechanism via conjunction of experimental/theoretical calculation. Structural reconstruction and heteroatom doping (especially oxygen or nitrogen doping) of carbon catalysts are useful strategies to boost their $2e^-$ ORR catalytic performance. Continuous studies are encouraged to screen out other useful nonmetallic heteroatoms (co-)doping carbon materials. Non-noble metal and molecular complex catalysts are widely studied for electrochemical generation of $2e^-$ ORR. Optimizing the transition metal sites and functional supports/coordination ligands are crucial to regulate their catalytic active sites, conductivity, and mass transfer process. Additionally, more advanced technologies, such as high-throughput screening studies, post DFT calculation, advanced characterization techniques, and machine learning method, can be used to further screen out highly efficient catalysts and uncover the catalytic sites/catalytic mechanism. It is most likely that in the next years a proliferation of new/cheap/advanced catalysts may exhibit high electrocatalytic activity/selectivity and stability toward $2e^-$ ORR, where the complex mechanistic features can be mastered at the nanoscale.

iv) Application of producing H_2O_2 with $2e^-$ ORR

H_2O_2 as renewable and clean energy source is widely used as a versatile and nontoxic commodity chemical. Environmental concerns are set to increase the demand for H_2O_2 over the coming year. Electrogenesis of H_2O_2 via $2e^-$ ORR, has become an emerging research field because of its flexibility and sustainability. It can be widely applied in many fields, such as organic pollutants degradation, water treatment, bacteria killing and disinfection, and energy storage. However, there are still many environmental fields and energy fields remaining to be further developed and utilized, such as protection against marine fouling organisms and energy storage/conversion. There is the lack of reported information on these above application fields. In addition, most applications are highly dependent on the electro-Fenton process by using H_2O_2 to form $\cdot OH$. Therefore, developing novel application fields of H_2O_2 electrogeneration is necessary, which will not only trigger industrial interest for the development of new preparative schemes in conjunction with sustainability, but also realize on-site generation of H_2O_2 from $2e^-$ ORR for real-time field use. Future scrutiny is desired to improve the catalytic activity of catalysts in various acid/alkaline/neutral electrolytes. The development of on-site setups combined with electrochemical generation of H_2O_2 is also crucial to promote its practical application.

Acknowledgements

This work was supported by the Key Research Program of Frontier Sciences, Chinese Academy of Sciences (ZDBS-LY-DQC025), National Natural Science Foundation of China for Exploring Key Scientific Instrument (No. 41827805), and Shandong Key Laboratory of Corrosion Science. N.W. acknowledges the scholarship provided by the University of Chinese Academy of Sciences (UCAS).

Conflict of Interest

The authors declare no conflict of interest.

Keywords

application, catalytic mechanism, electrochemical catalysts, hydrogen peroxide, two-electron oxygen reduction reaction

Received: January 11, 2021
Revised: March 17, 2021
Published online: May 27, 2021

- [1] a) E. Brillas, I. Sires, M. A. Oturan, *Chem. Rev.* **2009**, *109*, 6570; b) R. Hage, A. Lienke, *Angew. Chem., Int. Ed.* **2006**, *45*, 206.
- [2] J. M. Campos-Martin, G. Blanco-Brieva, J. L. G. Fierro, *Angew. Chem., Int. Ed.* **2006**, *45*, 6962.
- [3] a) J. K. Edwards, B. Solsona, E. Ntainjua N, A. F. Carley, A. A. Herzog, C. J. Kiely, G. J. Hutchings, *Science* **2009**, *323*, 1037; b) C. Xia, Y. Xia, P. Zhu, L. Fan, H. Wang, *Science* **2019**, *366*, 226.
- [4] a) I. Yamanaka, T. Murayama, *Angew. Chem., Int. Ed.* **2008**, *120*, 1926; b) E. Jung, H. Shin, W. H. Antink, Y. E. Sung, T. Hyeon, *ACS Energy Lett.* **2020**, *5*, 1881.
- [5] a) A. Kulkarni, S. Siahrostami, A. Patel, J. K. Nørskov, *Chem. Rev.* **2018**, *118*, 2302; b) Y. Zhou, G. Chen, J. Zhang, *J. Mater. Chem. A* **2020**, *8*, 20849.
- [6] E. Berl, *Trans. Electrochem. Soc.* **1939**, *76*, 359.
- [7] M. N. Young, M. J. Links, S. C. Popat, B. E. Rittmann, C. I. Torres, *ChemSusChem* **2016**, *9*, 3345.
- [8] a) S. Yang, A. Verdager-Casadevall, L. Arnarson, L. Silvioli, V. Colic', R. Frydendal, J. Rossmeisl, I. Chorkendorff, I. E. Stephens, *ACS Catal.* **2018**, *8*, 4064; b) Y. Jiang, P. Ni, C. Chen, Y. Lu, P. Yang, B. Kong, A. Fisher, X. Wang, *Adv. Energy Mater.* **2018**, *8*, 1801909.
- [9] a) A. Verdager-Casadevall, D. Deiana, M. Karamad, S. Siahrostami, P. Malacrida, T. W. Hansen, J. Rossmeisl, I. Chorkendorff, I. E. Stephens, *Nano Lett.* **2014**, *14*, 1603; b) V. Viswanathan, H. A. Hansen, J. Rossmeisl, J. K. Nørskov, *J. Phys. Chem. Lett.* **2012**, *3*, 2948.
- [10] X. Tan, H. A. Tahini, S. C. Smith, *Mater. Horiz.* **2019**, *6*, 1409.
- [11] Z. W. Seh, J. Kibsgaard, C. F. Dickens, I. Chorkendorff, J. K. Nørskov, T. F. Jaramillo, *Science* **2017**, *355*, eaad4998.
- [12] X. Guo, S. Lin, J. Gu, S. Zhang, Z. Chen, S. Huang, *ACS Catal.* **2019**, *9*, 11042.
- [13] S. Siahrostami, A. Verdager-Casadevall, M. Karamad, D. Deiana, P. Malacrida, B. Wickman, M. Escudero-Escribano, E. Paoli, R. Frydendal, T. Hansen, I. Chorkendorff, I. Stephens, J. Rossmeisl, *Nat. Mater.* **2013**, *12*, 1137.
- [14] a) J. Zhang, H. Zhang, M. J. Cheng, Q. Lu, *Small* **2020**, *16*, 1902845; b) K. Zhao, Y. Su, X. Quan, Y. Liu, S. Chen, H. Yu, *J. Catal.* **2018**, *357*, 118.
- [15] a) Z. Lu, G. Chen, S. Siahrostami, Z. Chen, K. Liu, J. Xie, L. Liao, T. Wu, D. Lin, Y. Liu, T. Jaramillo, J. Nørskov, Y. Cui, *Nat. Catal.* **2018**, *1*, 156; b) S. L. Hooe, A. L. Rheingold, C. W. Machan, *J. Am. Chem. Soc.* **2017**, *140*, 3232.
- [16] Y. Sun, L. Silvioli, N. R. Sahraie, W. Ju, J. Li, A. Zitolo, S. Li, A. Bagger, L. Arnarson, X. Wang, T. Moeller, D. Bersmeier, J. Rossmeisl, F. Jaouen, P. Strasser, *J. Am. Chem. Soc.* **2019**, *141*, 12372.
- [17] J. Gao, H. Yang, X. Huang, S.-F. Hung, W. Cai, C. Jia, S. Miao, H. M. Chen, X. Yang, Y. Huang, T. Zhang, B. Liu, *Chem* **2020**, *6*, 658.
- [18] S. Yang, Y. J. Tak, J. Kim, A. Soon, H. Lee, *ACS Catal.* **2017**, *7*, 1301.
- [19] a) R. Adžić, A. Tripković, N. Marković, *J. Electroanal. Chem. Interfacial Electrochem.* **1983**, *150*, 79; b) J. S. Jirkovský, M. Halasa, D. J.

- Schiffirin, *Phys. Chem. Chem. Phys.* **2010**, *12*, 8042; c) D. C. Ford, A. U. Nilekar, Y. Xu, M. Mavrikakis, *Surf. Sci.* **2010**, *604*, 1565; d) Y. Lu, Y. Jiang, X. Gao, W. Chen, *Chem. Commun.* **2014**, *50*, 8464.
- [20] Q. Chang, P. Zhang, A. H. B. Mostaghimi, X. Zhao, S. R. Denny, J. H. Lee, H. Gao, Y. Zhang, H. L. Xin, S. Siahrostami, J. Chen, Zh. Chen, *Nat. Commun.* **2020**, *11*, 2178.
- [21] Y. L. Wang, S. Gurses, N. Felvey, A. Boubnov, S. S. Mao, C. X. Kronawitter, *ACS Catal.* **2019**, *9*, 8453.
- [22] G. V. Fortunato, E. Pizzutilo, A. M. Mingers, O. Kasian, S. Cherevko, E. S. Cardoso, K. J. Mayrhofer, G. Maia, M. Ledendecker, *J. Phys. Chem. C* **2018**, *122*, 15878.
- [23] a) C. H. Choi, H. C. Kwon, S. Yook, H. Shin, H. Kim, M. Choi, *J. Phys. Chem. C* **2014**, *118*, 30063; b) C. H. Choi, M. Kim, H. C. Kwon, S. J. Cho, S. Yun, H.-T. Kim, K. J. Mayrhofer, H. Kim, M. Choi, *Nat. Commun.* **2016**, *7*, 10922.
- [24] J. S. Jirkovský, I. Panas, E. Ahlberg, M. Halasa, S. Romani, D. J. Schiffirin, *J. Am. Chem. Soc.* **2011**, *133*, 19432.
- [25] Z. Zheng, Y. H. Ng, D. W. Wang, R. Amal, *Adv. Mater.* **2016**, *28*, 9949.
- [26] a) Q. Shi, W. Zhu, H. Zhong, C. Zhu, H. Tian, J. Li, M. Xu, D. Su, X. Li, D. Liu, B. Xu, S. Beckman, D. Du, Y. Lin, *ACS Appl. Energy Mater.* **2019**, *2*, 7722; b) E. Pizzutilo, S. J. Freakley, S. Cherevko, S. Venkatesan, G. J. Hutchings, C. H. Liebscher, G. Dehm, K. J. Mayrhofer, *ACS Catal.* **2017**, *7*, 5699; c) E. Pizzutilo, O. Kasian, C. H. Choi, S. Cherevko, G. J. Hutchings, K. J. Mayrhofer, S. J. Freakley, *Chem. Phys. Lett.* **2017**, *683*, 436.
- [27] A. von Weber, E. T. Baxter, H. S. White, S. L. Anderson, *J. Phys. Chem. C* **2015**, *119*, 11160.
- [28] S. Yang, J. Kim, Y. J. Tak, A. Soon, H. Lee, *Angew. Chem., Int. Ed.* **2016**, *55*, 2058.
- [29] S. C. Perry, D. Pangotra, L. Vieira, L.-I. Csepei, F. C. Walsh, *Nat. Rev. Chem.* **2019**, *3*, 442.
- [30] W. P. Mounfield III, A. Garg, Y. Shao-Horn, Y. Román-Leshkov, *Chem* **2018**, *4*, 18.
- [31] H. Luo, C. Li, C. Wu, X. Dong, *RSC Adv.* **2015**, *5*, 65227.
- [32] Y.-L. Wang, S.-S. Li, X.-H. Yang, G.-Y. Xu, Z.-C. Zhu, P. Chen, S.-Q. Li, *J. Mater. Chem. A* **2019**, *7*, 21329.
- [33] a) V. Čolić, S. Yang, Z. Révay, I. E. Stephens, I. Chorkendorff, *Electrochim. Acta* **2018**, *272*, 192; b) H. Zhang, Y. Li, Y. Zhao, G. Li, F. Zhang, *ACS Appl. Mater. Interfaces* **2019**, *11*, 27846; c) Y. Sheng, S. Song, X. Wang, L. Song, C. Wang, H. Sun, X. Niu, *Electrochim. Acta* **2011**, *56*, 8651.
- [34] a) M. Assumpção, R. De Souza, D. Rascio, J. Silva, M. Calegario, I. Gaubeur, T. Paixão, P. Hammer, M. Lanza, M. C. d. Santos, *Carbon* **2011**, *49*, 2842; b) W. R. Barros, T. Ereno, A. C. Tavares, M. R. Lanza, *ChemElectroChem* **2015**, *2*, 714.
- [35] a) W. Yang, M. Zhou, J. Cai, L. Liang, G. Ren, L. Jiang, *J. Mater. Chem. A* **2017**, *5*, 8070; b) F. Yu, M. Zhou, X. Yu, *Electrochim. Acta* **2015**, *163*, 182; c) J. Miao, H. Zhu, Y. Tang, Y. Chen, P. Wan, *Chem. Eng. J.* **2014**, *250*, 312.
- [36] J. C. Byers, A. G. Güell, P. R. Unwin, *J. Am. Chem. Soc.* **2014**, *136*, 11252.
- [37] Y. Liu, X. Quan, X. Fan, H. Wang, S. Chen, *Angew. Chem., Int. Ed.* **2015**, *54*, 6837.
- [38] a) R. B. Valim, R. M. Reis, P. S. Castro, A. S. Lima, R. S. Rocha, M. Bertotti, M. R. Lanza, *Carbon* **2013**, *61*, 236; b) J. Moreira, V. B. Lima, L. A. Goulart, M. R. Lanza, *Appl. Catal., B* **2019**, *248*, 95.
- [39] a) T.-P. Fellinger, F. d. r. Hasché, P. Strasser, M. Antonietti, *J. Am. Chem. Soc.* **2012**, *134*, 4072; b) Y. Sun, I. Sinev, W. Ju, A. Bergmann, S. r. Dresp, S. Kühl, C. Spöri, H. Schmies, H. Wang, D. Bernsmeier, B. Paul, R. Schmack, R. Kraehnert, B. Cuenya, P. Strasser, *ACS Catal.* **2018**, *8*, 2844.
- [40] a) S. Chen, Z. Chen, S. Siahrostami, D. Higgins, D. Nordlund, D. Sokaras, T. R. Kim, Y. Liu, X. Yan, E. Nilsson, R. Sinclair, J. Nørskov, T. Jaramillo, Zh. Bao, *J. Am. Chem. Soc.* **2018**, *140*, 7851; b) D. Iglecias, A. Giuliani, M. Melchionna, S. Marchesan, A. Criado, L. Nasi, M. Bevilacqua, C. Tavagnacco, F. Vizza, M. Prato, P. Fornasiero, *Chem* **2018**, *4*, 106; c) H.-X. Zhang, S.-C. Yang, Y.-L. Wang, J.-C. Xi, J.-C. Huang, J.-F. Li, P. Chen, R. Jia, *Electrochim. Acta* **2019**, *308*, 74; d) L. Roldán, L. Truong-Phuoc, A. Ansón-Casaos, C. Pham-Huu, E. García-Bordejé, *Catal. Today* **2018**, *301*, 2; e) V. Perazzolo, C. Durante, R. Pilot, A. Paduano, J. Zheng, G. A. Rizzi, A. Martucci, G. Granozzi, A. Gennaro, *Carbon* **2015**, *95*, 949; f) G. Chen, J. Liu, Q. Li, P. Guan, X. Yu, L. Xing, J. Zhang, R. Che, *Nano Res.* **2019**, *12*, 2614; g) P. Su, M. Zhou, X. Lu, W. Yang, G. Ren, J. Cai, *Appl. Catal., B* **2019**, *245*, 583.
- [41] Z. Chen, S. Chen, S. Siahrostami, P. Chakhranont, C. Hahn, D. Nordlund, S. Dimosthenis, J. K. Nørskov, Z. Bao, T. F. Jaramillo, *React. Chem. Eng.* **2017**, *2*, 239.
- [42] J. Zhu, X. Xiao, K. Zheng, F. Li, G. Ma, H.-C. Yao, X. Wang, Y. Chen, *Carbon* **2019**, *153*, 6.
- [43] S. Chen, Z. Chen, S. Siahrostami, T. R. Kim, D. Nordlund, D. Sokaras, S. Nowak, J. W. To, D. Higgins, R. Sinclair, T. Jaramillo, J. Nørskov, Zh. Bao, *ACS Sustainable Chem. Eng.* **2018**, *6*, 311.
- [44] J. Park, Y. Nabae, T. Hayakawa, M.-a. Kakimoto, *ACS Catal.* **2014**, *4*, 3749.
- [45] Y. J. Sa, J. H. Kim, S. H. Joo, *Angew. Chem., Int. Ed.* **2019**, *58*, 1100.
- [46] H. Zhao, X. Shen, Y. Chen, S.-N. Zhang, P. Gao, X. Zhen, X.-H. Li, G. Zhao, *Chem. Commun.* **2019**, *55*, 6173.
- [47] L. Han, Y. Sun, S. Li, C. Cheng, C. E. Halbig, P. Feicht, J. L. Hübner, P. Strasser, S. Eigler, *ACS Catal.* **2019**, *9*, 1283.
- [48] H. W. Kim, H. Park, J. S. Roh, J. E. Shin, T. H. Lee, L. Zhang, Y. H. Cho, H. W. Yoon, V. J. Bukas, J. Guo, H. Park, T. Han, B. McCloskey, *Chem. Mater.* **2019**, *31*, 3967.
- [49] N. Jia, T. Yang, S. Shi, X. Chen, Z. An, Y. Chen, S. Yin, P. Chen, *ACS Sustainable Chem. Eng.* **2020**, *8*, 2883.
- [50] Y.-H. Lee, F. Li, K.-H. Chang, C.-C. Hu, T. Ohsaka, *Appl. Catal., B* **2012**, *126*, 208.
- [51] Y. Sun, S. Li, Z. P. Jovanov, D. Bernsmeier, H. Wang, B. Paul, X. Wang, S. Kühl, P. Strasser, *ChemSusChem* **2018**, *11*, 3388.
- [52] J. Zhang, G. Zhang, S. Jin, Y. Zhou, Q. Ji, H. Lan, H. Liu, J. Qu, *Carbon* **2020**, *163*, 154.
- [53] X. Yin, L. Lin, U. Martinez, P. Zelenay, *ACS Appl. Energy Mater.* **2019**, *2*, 7272.
- [54] X. Sheng, N. Daems, B. Geboes, M. Kurttepel, S. Bals, T. Breugelmanns, A. Hubin, I. F. Vankelecom, P. P. Pescarmona, *Appl. Catal., B* **2015**, *176*, 212.
- [55] H. W. Kim, M. B. Ross, N. Kornienko, L. Zhang, J. Guo, P. Yang, B. D. McCloskey, *Nat. Catal.* **2018**, *1*, 282.
- [56] Y. Yang, F. He, Y. Shen, X. Chen, H. Mei, S. Liu, Y. Zhang, *Chem. Commun.* **2017**, *53*, 9994.
- [57] D. San Roman, D. Krishnamurthy, R. Garg, H. Hafiz, M. Lamparski, N. T. Nuhfer, V. Meunier, V. Viswanathan, T. Cohen-Karni, *ACS Catal.* **2020**, *10*, 1993.
- [58] a) A. Moraes, M. Assumpção, F. Simões, V. Antonin, M. Lanza, P. Hammer, M. Santos, *Electrocatalysis* **2016**, *7*, 60; b) C. Y. Chen, C. Tang, H. F. Wang, C. M. Chen, X. Zhang, X. Huang, Q. Zhang, *ChemSusChem* **2016**, *9*, 1194; c) L. R. Aveiro, A. G. da Silva, V. S. Antonin, E. G. Candido, L. S. Parreira, R. S. Geonmonond, I. C. de Freitas, M. R. Lanza, P. H. Camargo, M. C. Santos, *Electrochim. Acta* **2018**, *268*, 101.
- [59] K.-H. Wu, D. Wang, X. Lu, X. Zhang, Z. Xie, Y. Liu, B.-J. Su, J.-M. Chen, D.-S. Su, W. Qi, Sh. Guo, *Chem* **2020**, *6*, 1443.
- [60] Y. Zhu, S. Qiu, F. Ma, G. Li, F. Deng, Y. Zheng, *Electrochim. Acta* **2018**, *261*, 375.
- [61] P. Wu, P. Du, H. Zhang, C. Cai, *Phys. Chem. Chem. Phys.* **2013**, *15*, 6920.

- [62] a) A. Asghar, A. A. A. Raman, W. M. A. W. Daud, A. Ramalingam, S. B. Zain, *Res. Chem. Intermed.* **2019**, *45*, 3311; b) L. Lai, J. R. Potts, D. Zhan, L. Wang, C. K. Poh, C. Tang, H. Gong, Z. Shen, J. Lin, R. S. Ruoff, *Energy Environ. Sci.* **2012**, *5*, 7936; c) T. Ikeda, M. Boero, S.-F. Huang, K. Terakura, M. Oshima, J.-i. Ozaki, *J. Phys. Chem. C* **2008**, *112*, 14706; d) E. Contreras, D. Dominguez, H. Tiznado, J. Guerrero-Sanchez, N. Takeuchi, G. Alonso-Nunez, O. E. Contreras, M. T. Oropeza-Guzmán, J. M. Romo-Herrera, *Nanoscale* **2019**, *11*, 2829.
- [63] R. A. Sidik, A. B. Anderson, N. P. Subramanian, S. P. Kumaraguru, B. N. Popov, *J. Phys. Chem. B* **2006**, *110*, 1787.
- [64] E. Chen, M. Bevilacqua, C. Tavagnacco, T. Montini, C.-M. Yang, P. Fornasiero, *Catal. Today* **2020**, *356*, 132.
- [65] B. Q. Li, C. X. Zhao, J. N. Liu, Q. Zhang, *Adv. Mater.* **2019**, *31*, 1808173.
- [66] B. W. Noffke, Q. Li, K. Raghavachari, L.-s. Li, *J. Am. Chem. Soc.* **2016**, *138*, 13923.
- [67] X. Xiao, T. Wang, J. Bai, F. Li, T. Ma, Y. Chen, *ACS Appl. Mater. Interfaces* **2018**, *10*, 42534.
- [68] a) M. H. M. T. Assumpção, A. Moraes, R. De Souza, M. Calegari, M. Lanza, E. Leite, M. Cordeiro, P. Hammer, M. C. d. Santos, *Electrochim. Acta* **2013**, *111*, 339; b) M. H. M. T. Assumpcao, A. Moraes, R. F. B. De Souza, I. Gaubeur, R. T. S. Oliveira, V. S. Antonin, G. R. P. Malpass, R. S. Rocha, M. L. Calegari, M. R. V. Lanza, *Appl. Catal., A* **2012**, *411*, 1.
- [69] V. Antonin, M. Assumpção, J. Silva, L. Parreira, M. Lanza, M. Santos, *Electrochim. Acta* **2013**, *109*, 245.
- [70] F. V. dos Reis, V. S. Antonin, P. Hammer, M. C. Santos, P. H. Camargo, *J. Catal.* **2015**, *326*, 100.
- [71] P. Simas, V. Antonin, L. Parreira, P. Hammer, F. Silva, M. Kronka, R. Valim, M. R. d. V. Lanza, M. Santos, *Electrocatalysis* **2017**, *8*, 311.
- [72] V. S. Pinheiro, E. C. Paz, L. R. Aveiro, L. S. Parreira, F. M. Souza, P. H. Camargo, M. C. Santos, *Electrochim. Acta* **2018**, *259*, 865.
- [73] J. F. Carneiro, L. C. Trevelin, A. S. Lima, G. N. Meloni, M. Bertotti, P. Hammer, R. Bertazzoli, M. R. Lanza, *Electrocatalysis* **2017**, *8*, 189.
- [74] R. Liu, L. Ran, B. Niu, Y. Wei, *J. Nanosci. Nanotechnol.* **2018**, *18*, 4667.
- [75] J. F. Carneiro, M. J. Paulo, M. Siaj, A. C. Tavares, M. R. Lanza, *Chem-ElectroChem* **2017**, *4*, 508.
- [76] N. Wang, S. Ma, J. Duan, X. Zhai, F. Guan, X. Wang, B. Hou, *Electrochim. Acta* **2020**, *340*, 135880.
- [77] a) X.-b. Gong, Z. Yang, L. Peng, A.-l. Zhou, Y.-l. Liu, Y. Liu, *J. Power Sources* **2018**, *378*, 190; b) X. Cheng, S. Dou, G. Qin, B. Wang, P. Yan, T. T. Isimjan, X. Yang, *Int. J. Hydrogen Energy* **2020**, *45*, 6128; c) S. Marcotte, D. Villers, N. Guillet, L. Roue, J. Dodelet, *Electrochim. Acta* **2004**, *50*, 179; d) A. Bonakdarpour, D. Esau, H. Cheng, A. Wang, E. Gyenge, D. P. Wilkinson, *Electrochim. Acta* **2011**, *56*, 9074; e) I. Yamanaka, R. Ichihashi, T. Iwasaki, N. Nishimura, T. Murayama, W. Ueda, S. Takenaka, *Electrochim. Acta* **2013**, *108*, 321.
- [78] J. Biemolt, K. van der Veen, N. J. Geels, G. Rothenberg, N. Yan, *Carbon* **2019**, *155*, 643.
- [79] C. H. Choi, W. S. Choi, O. Kasian, A. K. Mechler, M. T. Sougrati, S. Brüller, K. Strickland, Q. Jia, S. Mukerjee, K. J. Mayrhofer, F. Jaouen, *Angew. Chem., Int. Ed.* **2017**, *56*, 8809.
- [80] J. F. Carneiro, M. J. Paulo, M. Siaj, A. C. Tavares, M. R. Lanza, *J. Catal.* **2015**, *332*, 51.
- [81] M. Assumpcao, D. Rascio, J. Ladeia, R. De Souza, E. T. Neto, M. Calegari, R. Oliveira, I. Gaubeur, M. Lanza, M. Santos, *Int. J. Electrochem. Sci.* **2011**, *6*, 1586.
- [82] H. Sheng, E. D. Hermes, X. Yang, D. Ying, A. N. Janes, W. Li, J. Schmidt, S. Jin, *ACS Catal.* **2019**, *9*, 8433.
- [83] A. Lenarda, M. Bevilacqua, C. Tavagnacco, L. Nasi, A. Criado, F. Vizza, M. Melchionna, M. Prato, P. Fornasiero, *ChemSusChem* **2019**, *12*, 1664.
- [84] W. R. Barros, Q. Wei, G. Zhang, S. Sun, M. R. Lanza, A. C. Tavares, *Electrochim. Acta* **2015**, *162*, 263.
- [85] M. Suk, M. W. Chung, M. H. Han, H.-S. Oh, C. H. Choi, *Catal. Today* **2021**, *359*, 99.
- [86] C. Tang, Y. Jiao, B. Shi, Q. Zhang, S. Qiao, *Angew. Chem., Int. Ed.* **2020**, *59*, 9171.
- [87] R.-Q. Zhang, T.-H. Lee, B.-D. Yu, C. Stampfl, A. Soon, *Phys. Chem. Chem. Phys.* **2012**, *14*, 16552.
- [88] K. Jjiang, S. Back, A. J. Akey, C. Xia, Y. Hu, W. Liang, D. Schaak, E. Stavitski, J. K. Nørskov, S. Siahrostami, H. Wang, *Nat. Commun.* **2019**, *10*, 3997.
- [89] J. Zhang, H. Yang, J. Gao, S. Xi, B. Liu, *Carbon Energy* **2020**, *2*, 276.
- [90] a) N. Oyama, N. Oki, H. Ohno, Y. Ohnuki, H. Matsuda, E. Tsuchida, *J. Phys. Chem.* **1983**, *87*, 3642; b) K. Tammeveski, K. Kontturi, R. J. Nichols, R. J. Potter, D. J. Schiffrin, *J. Electroanal. Chem.* **2001**, *515*, 101; c) I. Hatay, B. Su, M. A. Méndez, C. Corminboeuf, T. Khoury, C. P. Gros, M. Bourdillon, M. Meyer, J.-M. Barbe, M. Ersoz, S. Zalis, Z. Samec, H. Girault, *J. Am. Chem. Soc.* **2010**, *132*, 13733; d) V. Briega-Martos, A. Ferre-Vilaplana, A. de la Peña, J. L. Segura, F. Zamora, J. M. Feliu, E. Herrero, *ACS Catal.* **2017**, *7*, 1015.
- [91] A. Bettelheim, T. Kuwana, *Anal. Chem.* **1979**, *51*, 2257.
- [92] T. Sawaguchi, T. Matsue, K. Itaya, I. Uchida, *Electrochim. Acta* **1991**, *36*, 703.
- [93] Z. Halime, H. Kotani, Y. Li, S. Fukuzumi, K. D. Karlin, *Proc. Natl. Acad. Sci. USA* **2011**, *108*, 13990.
- [94] a) I. Creaser, R. Geue, J. M. Harrowfield, A. Herlt, A. Sargeson, M. Snow, J. Springborg, *J. Am. Chem. Soc.* **1982**, *104*, 6016; b) Y. Yamada, Y. Fukunishi, S.-i. Yamazaki, S. Fukuzumi, *Chem. Commun.* **2010**, *46*, 7334; c) S. Sun, N. Jjiang, D. Xia, *J. Phys. Chem. C* **2011**, *115*, 9511.
- [95] P. T. Smith, Y. Kim, B. P. Benke, K. Kim, C. J. Chang, *Angew. Chem., Int. Ed.* **2020**, *59*, 4902.
- [96] N. U. Day, C. C. Wamser, *J. Phys. Chem. C* **2017**, *121*, 11076.
- [97] a) B. H. Solis, S. Hammes-Schiffer, *Inorg. Chem.* **2014**, *53*, 6427; b) C. W. Anson, S. Ghosh, S. Hammes-Schiffer, S. S. Stahl, *J. Am. Chem. Soc.* **2016**, *138*, 4186; c) C. W. Anson, S. S. Stahl, *J. Am. Chem. Soc.* **2017**, *139*, 18472.
- [98] Y.-H. Wang, M. L. Pegis, J. M. Mayer, S. S. Stahl, *J. Am. Chem. Soc.* **2017**, *139*, 16458.
- [99] a) N. Kobayashi, H. Saiki, T. Osa, *Chem. Lett.* **1985**, *14*, 1917; b) J. Masa, K. Ozoemena, W. Schuhmann, J. H. Zagal, *J. Porphyrins Phthalocyanines* **2012**, *16*, 761; c) W. Schöfberger, F. Faschinger, S. Chattopadhyay, S. Bhakta, B. Mondal, J. A. Elemans, S. Müllegger, S. Tebi, R. Koch, F. Klappenberger, *Angew. Chem., Int. Ed.* **2016**, *55*, 2350.
- [100] S. L. Hooe, C. W. Machan, *J. Am. Chem. Soc.* **2019**, *141*, 4379.
- [101] E. Mitraka, M. Gryszel, M. Vagin, M. J. Jafari, A. Singh, M. Warczak, M. Mitrakas, M. Berggren, T. Ederth, I. Zozoulenko, *Adv. Sustainable Syst.* **2019**, *3*, 1800110.
- [102] M. Warczak, M. Gryszel, M. Jakešová, V. Ďerek, E. D. Głowacki, *Chem. Commun.* **2018**, *54*, 1960.
- [103] L.-Z. Peng, P. Liu, Q.-Q. Cheng, W.-J. Hu, Y. A. Liu, J.-S. Li, B. Jjiang, X.-S. Jia, H. Yang, K. Wen, *Chem. Commun.* **2018**, *54*, 4433.
- [104] F. Yu, M. Zhou, L. Zhou, R. Peng, *Environ. Sci. Technol. Lett.* **2014**, *1*, 320.
- [105] a) S. Yuan, N. Gou, A. N. Alshawabkeh, A. Z. Gu, *Chemosphere* **2013**, *93*, 2796; b) Y. Xiang, J. Fang, C. Shang, *Water Res.* **2016**, *90*, 301.
- [106] H. Zhao, L. Qian, Y. Chen, Q. Wang, G. Zhao, *Chem. Eng. J.* **2018**, *332*, 486.
- [107] a) A. Reyes-Cruzaley, R. Félix-Navarro, B. Trujillo-Navarrete, C. Silva-Carrillo, J. Zapata-Fernández, J. Romo-Herrera, O. Contreras, E. Reynoso-Soto, *Electrochim. Acta* **2019**, *296*, 575; b) L. Fu, S.-J. You, G.-q. Zhang, F.-L. Yang, X.-h. Fang, *Chem. Eng. J.* **2010**, *160*, 164.

- [108] a) Y. Liu, J. Xie, C. N. Ong, C. D. Vecitis, Z. Zhou, *Environ. Sci. Water Res. Technol.* **2015**, *1*, 769; b) Y.-J. Ko, H.-G. Kim, M. G. Seid, K. Cho, J.-W. Choi, W.-S. Lee, S. W. Hong, *ACS Sustainable Chem. Eng.* **2018**, *6*, 14857; c) L. Li, H. Hu, X. Teng, Y. Yu, Y. Zhu, X. Su, *Chem. Eng. Process.* **2018**, *133*, 34.
- [109] A. Asghar, A. A. Raman, W. M. A. W. Daud, *J. Chem. Technol. Biotechnol.* **2017**, *92*, 1825.
- [110] a) T. X. H. Le, R. Esmilaire, M. Drobek, M. Bechelany, C. Vallicari, D. L. Nguyen, A. Julbe, S. Tingry, M. Cretin, *J. Mater. Chem. A* **2016**, *4*, 17686; b) H. Huang, C. Han, G. Wang, C. Feng, *Electrochim. Acta* **2018**, *259*, 637.
- [111] W. Wang, J. Yu, J. Zou, X. Yu, *Electrochim. Acta* **2016**, *191*, 426.
- [112] C. Ridruejo, F. Alcaide, G. Álvarez, E. Brillas, I. Sirés, *J. Electroanal. Chem.* **2018**, *808*, 364.
- [113] a) W. Zhou, J. Gao, Y. Ding, H. Zhao, X. Meng, Y. Wang, K. Kou, Y. Xu, S. Wu, Y. Qin, *Chem. Eng. J.* **2018**, *338*, 709; b) W. Zhou, X. Meng, L. Rajic, Y. Xue, S. Chen, Y. Ding, K. Kou, Y. Wang, J. Gao, Y. Qin, *Electrochem. Commun.* **2018**, *96*, 37.
- [114] H. Kim, J. Lim, S. Lee, H.-H. Kim, C. Lee, J. Lee, W. Choi, *Environ. Sci. Technol.* **2019**, *53*, 2918.
- [115] B.-C. Huang, J. Jiang, W.-K. Wang, W.-W. Li, F. Zhang, H. Jiang, H.-Q. Yu, *ACS Sustainable Chem. Eng.* **2018**, *6*, 5540.
- [116] N. Tan, Z. Yang, X.-b. Gong, Z.-r. Wang, T. Fu, Y. Liu, *Sci. Total Environ.* **2019**, *650*, 2567.
- [117] a) L. Wang, M. Cao, Z. Ai, L. Zhang, *Environ. Sci. Technol.* **2015**, *49*, 3032; b) G. Ren, M. Zhou, M. Liu, L. Ma, H. Yang, *Chem. Eng. J.* **2016**, *298*, 55.
- [118] T. Lian, C. Huang, F. Liang, X. Li, J. Xi, *ACS Appl. Mater. Interfaces* **2019**, *11*, 45692.
- [119] X. Li, F. Liu, W. Zhang, H. Lu, J. Zhang, *Environ. Pollut.* **2019**, *254*, 112958.
- [120] P. J. Alvarez, C. K. Chan, M. Elimelech, N. J. Halas, D. Villagrán, *Nat. Nanotechnol.* **2018**, *13*, 634.
- [121] S. Fukuzumi, Y. Yamada, K. D. Karlin, *Electrochim. Acta* **2012**, *82*, 493.
- [122] W. Wang, Y. Hu, Y. Liu, Z. Zheng, S. Chen, *ACS Appl. Mater. Interfaces* **2018**, *10*, 31855.



Nan Wang is currently a postdoctoral fellow at Institute of Oceanology, Chinese Academy of Sciences. She received her Ph.D. in Institute of Oceanology, Chinese Academy of Sciences in 2020 under the supervision of Prof. Jizhou Duan and had been a visiting scholar at the University of California, Irvine in USA (2019–2020). Her research interests focus on electrochemical H₂O₂ generation for in situ marine biological fouling protection.



Shaobo Ma is currently a Ph. D candidate at Harbin Institute of Technology under the supervision of Prof. Pengjian Zuo. He received master's degree at in Dalian University of Technology in 2016, and had been a visiting scholar at University of California, Irvine in USA (2019–2020). His current research interests focus on energy materials in Li-ion/metal batteries and electrochemical catalysts in fuel cells.



Pengjian Zuo is currently a professor in School of Chemistry and Chemical Engineering at Harbin Institute of Technology (HIT). He received the B.E. and Ph.D. degree in Chemical Engineering and Technology at HIT in 2002 and 2007, respectively. He was a visiting scholar at Pacific Northwest National Laboratory in 2012–2013. His research interests focus on energy storage materials and high-performance energy storage/conversion systems including lithium/sodium ion batteries, lithium/magnesium sulfur batteries, and lithium metal batteries.



Jizhou Duan is currently a full professor in the Institute of Oceanology, Chinese Academy of Sciences. He received his Ph.D. from Institute of Oceanology, Chinese Academy of Sciences in 2003. He then worked as a visiting associate in the Tokyo Institute of Technology (2003–2004) and the University of Hong Kong (2009), respectively. His research interests include marine corrosion and protection technology.



Baorong Hou is an academican at Chinese Academy of Engineering. He received the B.E. and Ph.D. degree from Fudan University in 1967 and Tokyo Institute of Technology in 1994, respectively. His research interests include marine corrosion and protection technology, Marine engineering cathodic protection monitoring technology, stray current monitoring and control technology, new composite sacrificial anode technology, marine biological corrosion, pollution prevention technology etc.